REDUCTION OF OFF-BORESIGHT FIELDS
FOR A TEM HORN ANTENNA

THESIS
Dennis J. Wolstenholme
Second Lieutenant, USAF

AFIT/GE/ENG/94D-33

DEPARTMENT OF THE AIR FORCE
AIR UNIVERSITY
AIR FORCE INSTITUTE OF TECHNOLOGY

Wright-Patterson Air Force Base, Ohio

19941228 093

ADA289708

REDUCTION OF OFF-BORESIGHT FIELDS
FOR A TEM HORN ANTENNA

THESIS
Dennis J. Wolstenholme
Second Lieutenant, USAF

AFIT/GE/ENG/94D-33

DTIC QUALITY INSPECTED **8**

REPORT DOCUMENTATION PAGE

1 AGENCY USE ONLY (Leave blank)	2. REPORT DATE	3. REPORT TYPE AND DATES COVERED
	December 1994	Master's Thesis

4. TITLE AND SUBTITLE
Reduction of Off-Boresight Fields for a TEM Horn Antenna

5 FUNDING NUMBERS

6. AUTHOR(S)
Dennis J. Wolstenholme

7. PERFORMING ORGANIZATION NAME(S) AND ADDRESS(ES)
Air Force Institute of Technology, WPAFB OH 45433-6583

8 PERFORMING ORGANIZATION REPORT NUMBER
AFIT/GE/ENG/94D-33

9. SPONSORING/MONITORING AGENCY NAME(S) AND ADDRESS(ES)
Capt. J. Raley Marek
USAF Phillips Laboratory
PL/WSR
Kirtland AFB, NM 87117

10 SPONSORING/MONITORING AGENCY REPORT NUMBER

11. SUPPLEMENTARY NOTES

12a. DISTRIBUTION/AVAILABILITY STATEMENT

Distribution Unlimited

12b DISTRIBUTION CODE

13. ABSTRACT (Maximum 200 words)

Abstract

This research involves the design, modeling, and testing of both tapered periodic surfaces (TPS) and transverse electromagnetic (TEM) horns. The goal is to reduce the off-boresight fields for a TEM horn and increase the peak-to-peak field levels on boresight. This is accomplished by applying a TPS to the free space end. Two tapers are designed - one that approximates an exponential impedance function and one that approximates a triangular impedance function. Both reduce the off-boresight fields of the TEM horn. In most cases the exponential taper reduces the field levels further than the triangular taper. This research shows that a TPS is an effective method of reducing diffraction. A procedure for designing a TPS to approximate a specific impedance function is presented. A two-dimensional finite difference time domain (FDTD) model predicts the tapers will reduce the diffraction. Experimental results verify the TPS's ability to reduce the peak off-boresight fields for a TEM horn antenna.

14. SUBJECT TERMS
TEM Horn, Transient Electromagnetics, Tapered Periodic Surfaces

15 NUMBER OF PAGES
178

16. PRICE CODE

17. SECURITY CLASSIFICATION OF REPORT	18. SECURITY CLASSIFICATION OF THIS PAGE	19. SECURITY CLASSIFICATION OF ABSTRACT	20 LIMITATION OF ABSTRACT
UNCLASSIFIED	UNCLASSIFIED	UNCLASSIFIED	UL

REDUCTION OF OFF-BORESIGHT FIELDS
FOR A TEM HORN ANTENNA

THESIS

Presented to the Faculty of the School of Engineering

of the Air Force Institute of Technology

Air Education and Training Command (AETC)

In Partial Fulfillment of the

Requirements for the Purpose of

Master of Science in Electrical Engineering

Dennis J. Wolstenholme, B.S.

Second Lieutenant, USAF

December 1994

Accession For	
NTIS GRA&I	☑
DTIC TAB	☐
Unannounced	☐
Justification	
By	
Distribution/	
Availability Codes	
Dist	Avail and/or Special
A-1	

Approved for public release; distribution unlimited

ii

Preface

The purpose of this study was to reduce the off-boresight fields for a transverse electromagnetic (TEM) horn antenna over a bandwidth of 20:1. A second goal was to maximize the on-boresight fields over the same bandwidth. These goals were met by applying tapered periodic surfaces (TPSs) to the free space ends of the horn. The TPS reduced the diffraction that causes the off-boresight field levels.

A design of both a TEM horn and TPS was performed. After completion of the designs, they were modeled on using an electromagnetic code to ensure their performance. Then the tapers and horn was built and tested to verify the computer predictions.

As with all scientific work, this thesis would not have been possible without the assistance of many individuals. I would like to take some time and recognize those that helped me with this thesis. I would like to thank First Lieutenant Russell A. Burleson for his help throughout the research. He was instrumental in my understanding of the topic and graciously volunteered his time to review my work. Drs. Errol English and Steve Miller, of Mission Research Corporation, were very helpful in the manufacturing of the tapers in an extraordinarily short amount of time. I would also like to thank Dr. Gerald Buccenhauer at Phillips Laboratory for all the help building the test setup at the High Energy Research and Test Facility. My sponsors, Captain J. Raley Marek of Phillips Laboratory and Major Dennis Andersh of Wright Laboratory, were very helpful in preparing the test facilities and providing the funding for the research. I would like to thank my thesis advisor Dr. Andrew Terzuoli for his guidance and assistance throughout the thesis research. I would also like to thank my thesis committee members Major Gerald Gerace, Captain J. Paul Skinner, and Captain Joseph Sacchini for their time and consideration. I want to recognize my fellow AFIT classmates for keeping me sane through the whole process. Finally, I would like to thank my parents for reviewing my work and offering support and encouragement whenever possible.

Dennis J. Wolstenholme

iii

Table of Contents

ADA289788

List of Figures

List of Tables

List of Abbreviations

EM...electromagnetic
FDTD...finite difference time domain
MRC...Mission Research Corporation
PMM...periodic moment method
RCS...radar cross section
TE...transverse electric
TEM...transverse electromagnetic
TM...transverse magnetic
TPS...tapered periodic surface
UWB...ultra-wideband

Abstract

This research involves the design, modeling, and testing of both tapered periodic surfaces (TPS) and transverse electromagnetic (TEM) horns. The goal is to reduce the off-boresight fields for a TEM horn and increase the peak-to-peak field levels on boresight. This is accomplished by applying a TPS to the free space end. Two tapers are designed — one that approximates an exponential impedance function and one that approximates a triangular impedance function. Both reduce the off-boresight fields of a TEM horn. In most cases the exponential taper reduces the field levels further than the triangular taper. This research shows that a TPS is an effective method of reducing diffraction. A procedure for designing a TPS to approximate a specific impedance function is presented. A two-dimensional finite difference time domain (FDTD) model predicts the tapers will reduce the diffraction. Experimental results verify the TPS's ability to reduce the fields for a TEM horn antenna

Reduction of Off-Boresight Fields
for a TEM Horn Antenna

Chapter 1: Introduction

There are many potential applications for ultra-wideband systems. Target recognition, collision avoidance, and detection through lossy materials (such as concrete) are some examples [1]. Wideband communication requires an antenna capable of undistorted transmission and reception of wideband signals High power, short pulse radiating systems also require ultra-wideband systems.

Ultra-wideband, short pulse radiation systems require broadband antennas with low dispersion characteristics. One such antenna, the transverse electromagnetic (TEM) horn, does not suffer from frequency dispersion like many other broadband antennas such as logarithmic and spiral antennas. The TEM horn radiates all the desired frequencies simultaneously, whereas, the logarithmic and spiral antennas radiate the high frequencies first and the low frequencies later.

Unfortunately, the abrupt transition from the conductors of a TEM horn antenna to free space causes reflection and diffraction at the ends of the horn. This diffraction increases the off-boresight electric field strength. This research investigates the application of tapered periodic surfaces (TPS) to the ends of the antenna as a method to reduce the diffraction.

The purpose of this chapter is to provide a brief overview of the reduction of off-boresight fields for a TEM horn antenna. The objectives of this research and terminology used throughout the thesis are described in detail. A brief overview of the methodology used in this research is provided. The computer codes used in the design and modeling of the TEM horn and TPS are described. Finally, the major assumptions of the project are listed.

1

Objectives

This research topic has two main goals or objectives. The first goal is to reduce the off-boresight electric field levels for a TEM horn antenna. The second goal is to maximize the on-boresight peak-to-peak electric fields over a bandwidth of 20:1. These goals are met by applying a TPS to the ends of the horn.

Terminology

Many of these terms and topics in this thesis are relatively new to the area of antennas and electromagnetics, and therefore, require clarification.

Ultra-wideband (UWB) systems are an exciting development in the field of the electrical engineering. They offer many new features not available with more common narrow band systems. The main characteristic of an UWB system is that it operates over a wide band of frequencies. UWB systems operate by radiating short pulses in the time domain. This provides a wide spectrum in the frequency domain. It is not uncommon to develop UWB systems capable of operating with a bandwidth of 20:1. A UWB radiating system, therefore, requires an antenna that is able to perform over the same bandwidth. The operating bandwidth of the TEM horn antenna in this study is 300 MHz to 6 GHz.
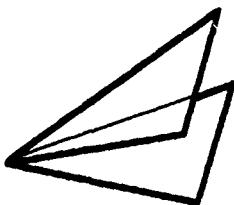
Figure 1. TEM Horn Antenna

2

A TEM horn antenna, shown in Figure 1, is a two-conductor, end-fire, traveling wave structure. With proper selection of the flare angle and plate widths, the TEM horn maintains a constant impedance and radiates only the TEM mode. The abrupt transition from the conductive elements of the TEM horn to free space causes some electromagnetic energy to diffract into the off-boresight directions.

Tapered periodic surfaces (TPS) ease the transition from conductors to free space. A TPS is a "lattice of wire or slot elements with progressively shorter lengths from one edge of the surface to the other" [2]. A wire TPS is shown in Figure 2. The TPS tapers from a low reactance (Z=0) to a high reactance (Z=±j∞). Since the impedance transitions gradually, the diffraction reduces.

ground
plane

free
space
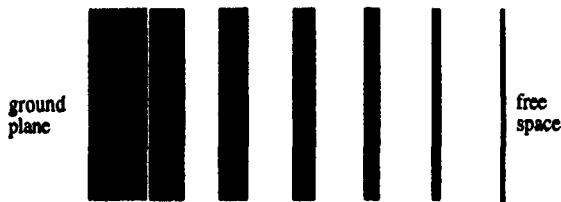
Figure 2. Wire Type of Tapered
Periodic Surface

Design Methodology

The design process of this research can be separated into two pieces — the design of a TEM horn antenna and the design of a TPS. The two pieces can be designed separately keeping in mind that the goal is to reduce the off-boresight fields for bandwidth of 300 MHz to 6 GHz.

In general, the design of a TEM horn requires selecting the length, width at the aperture, and flare angle between the plates. The parameters are adjusted to meet the four design criteria for an ultra-wideband, short pulse radiating system. The design criteria are·

3

1) a constant amplitude response, 2) a linear phase response, 3) no reflections or resonances along the conductors, and 4) a wide bandwidth. The actual design equations are presented in later chapters.

After the TEM horn design is complete, a finite difference time domain (FDTD) computer code models the horn. The FDTD code analyzes the TEM horn before production and testing. The FDTD code can only approximate the horn geometry. Therefore, the results of the modeling are not the exact response of the TEM horn. However, the effects of definitive parameters can be analyzed.

The TPS design process is quite involved. A periodic moment method (PMM) computer code models each of the TPS elements. The code computes the reflection coefficient for a doubly infinite array involving each element versus frequency. From the reflection coefficient, a transmission line model determines the sheet impedance. The final TPS geometry is then determined by approximating a known impedance function.

After the proper geometry is determined, a two-dimensional FDTD code models a side view of the TPS. Computer limitations only allow the use of a two-dimensional FDTD code. This model demonstrates the reduction of field levels in the shadow region of the model.

After both the TEM horn and TPS designs are validated, the testing begins. Testing of the TEM horn and TPS attachments is performed at the High Energy Research and Test Facility of USAF Phillips Laboratory.

Description of Tools

As stated above, this research utilizes two different electromagnetic computer codes — a FDTD code and a PMM code. These codes have very different capabilities and applications, and therefore, they warrant further detailed description.

The primary validation tool in this research is a FDTD code by Luebbers [3], which has been thoroughly validated. The FDTD method relies on computing Maxwell's equations discretized in both time and space. A grid with the electric fields located on the

4

edges and the magnetic fields located on the faces models the object of interest. The fields are updated at every location in the test space as time progresses in discrete steps.

The main design tool for the TPS is a PMM code by Henderson [4]. The PMM methodology lies in a "plane wave expansion technique which allows each infinite array of scatterers to be modeled by a single element called the reference element" [4]. A periodic array infinite in length and width models each element of the TPS separately. The code calculates the reflection coefficient associated with the local environment around each element versus frequency.

Assumptions

The following assumptions are important to keep in mind.

Perfect Electric Conductors (PEC) and Lossless Dielectrics

All conductive materials are assumed to be perfect, implying the conductivity of the metal is very large and the resistivity of the metal is very small. For the copper materials used, the PEC assumption is reasonably accurate. The dielectric's properties are assumed lossless and independent of frequency over the frequency range of interest. Again with the glass epoxy materials in this study, the lossless and frequency independent assumptions are reasonable.

Two-Dimensional Tapered Periodic Surfaces

The TPSs are modeled as two-dimensional (2D) structures in FDTD. The strips are infinite in $\hat{z}$ direction; the actual elements are of course not 2D structures. The TPS is attached to the triangularly shaped TEM horn. The two-dimensional approximation does not represent the actual performance of the TPS, but it does demonstrate the reduction of the off-boresight field strength by the TPS.

Local Periodicity

The TPS elements are designed using a PMM code. In reality, the elements are not periodic; the gaps between the elements and the width of the strips change as a function of

5

length. However, from element to element the geometry does not change greatly, and the TPS can be considered locally periodic.

Summary

This chapter outlined the study to be presented in this thesis. The remaining chapters provide the details necessary for a complete understanding of the research. Chapter 2 reviews the previous work of other upon which this research is built. Chapter 3 describes the design, modeling, and testing of the TEM horn and TPS. The results of the modeling and testing are analyzed in the Chapter 4. Chapter 5 briefly recounts the results of the research and provides some suggestions for future work.

6

Chapter 2: Background

This chapter reviews the previous work of others relevant to this thesis. The general properties of an UWB system establishes the criteria that the design must meet. A TEM horn meets many of the UWB criteria; however, there are inherent deficiencies. The theory and application of TPS is presented as a solution to the limitations of a TEM horn.

Ultra-Wideband Systems

There are many potential uses for a UWB system. The advantage of a UWB system over a narrow band system is the ability to access a wide range of frequencies for a single purpose. However, the method of design and analysis must be reevaluated for a UWB system. Analysis of an UWB system in the frequency domain is a Herculean effort because of the large bandwidth of a UWB system. Therefore, many researchers have turned to time domain analysis. This study employs mostly time domain analysis.

In order to use an UWB system, a method of transmitting and receiving UWB signals must be found. An antenna capable of transmitting and receiving UWB signals must have the following characteristics: 1) a constant amplitude response, 2) a linear phase response, 3) no reflections or resonances, and 4) a wide bandwidth [5].

A constant amplitude response over the frequency range of interest is an important feature to any antenna. An antenna distorts a pulse when certain frequencies are attenuated more than others. In a communication system the distortion may be so severe that the information cannot be recognized.

A linear phase response is an important characteristic of a broadband antenna. Comparing a system with a linear phase response to a system with a non-linear phase response system demonstrates its importance [5]. Consider an pulse centered at time t=0. This pulse can be expressed as an infinite sum of cosine functions with weighting factors determined by a trigonometric Fourier series. If an antenna with a non-linear phase response radiates this pulse, some of the cosine functions are shifted in phase. Therefore, frequency dispersion occurs, and the pulse spreads in time. In a short pulse radiation

7

system, a phase dispersive antenna spreads the short pulse in time and ultimately transmits a long pulse.

Reflections occur at abrupt transitions, either physical changes or material changes. Therefore, a reflection can occur when the antenna geometry experiences a severe change in radius of curvature (a corner) or when the electrical properties of the material change rapidly (junction of two materials). Reflections in an antenna are also accompanied by diffraction. The electric fields travel the length of the antenna, reach a discontinuity, and partially reflect. An antenna transmits the energy that does not reflect. If the reflection is small, most of the transmitted energy moves in the direction of propagation. If the reflection is large, much of the transmitted energy scatters in all directions thereby decreasing the amount of energy in the desired direction. This scattering is known as diffraction. Since the purpose of an antenna is to direct energy, diffraction must be minimized. By providing a smooth transition from the low impedance of metal conductors to the high impedance of free space, an antenna minimizes reflections and, therefore, diffraction.

Wide bandwidth is the defining parameter for an UWB antenna. Generally speaking, a broadband antenna will be able to reproduce a signal over a 2:1 bandwidth [6]. While harder to define, an ultra-wideband antenna reproduces a signal over a 10:1 bandwidth or greater. The ability to reproduce signals without distortion defines bandwidth. Therefore, the bandwidth of an antenna is dependent upon its amplitude and phase response.

TEM Horn Antennas

In their search for a broadband antenna with low dispersion characteristics and high directivity many researchers turn to the TEM horn antenna. Again, a TEM horn antenna is a two-conductor, endfire traveling wave structure as shown in Figure 1. With proper selection of the flare angle, length of the conductors, and plate widths, the TEM horn maintains a constant impedance and radiates only the TEM mode. A design guide by Onderejka, Ladbury, and Medley describes the design process for a TEM horn [5]. In general, the design of a TEM horn requires selecting the geometrical parameters such that the four UWB criteria are satisfied. The design equations are outlined in Chapter 3.

8

The TEM horn, by its geometry, has a constant amplitude response. Two simple models represent a TEM horn — a high frequency model and a low frequency model [5].

At high frequencies, the TEM horn acts as a transmission line with a purely resistive load as shown in Figure 3. The response is obviously independent of frequency, and therefore, maintains the constant amplitude response criteria.
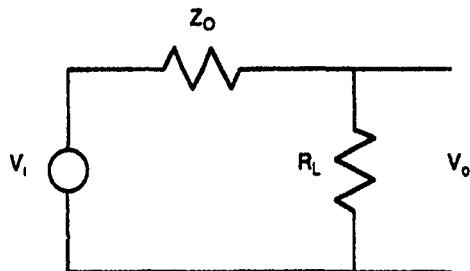
Figure 3. High Frequency Transmission Line
Model of a TEM Horn

For low frequencies, the TEM horn behaves as a short dipole. A transmission line can also model a short dipole. The antenna responds like a voltage source with a capacitive load as shown in Figure 4.
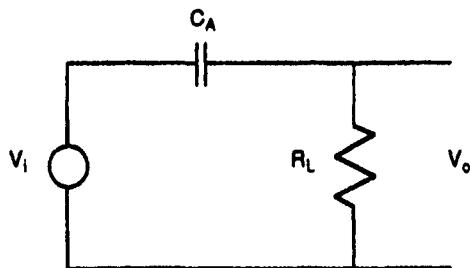
Figure 4. Low Frequency Transmission Line
Model of a TEM Horn

9

The amplitude response is similar to that of a simple RC filter in which the capacitance can be found by [5]

$$C_A = \frac{1}{2\omega R_L}.$$ (1)

Terminating the antenna with a capacitive load, as demonstrated in Figure 5, forces the response of the antenna to be independent of frequency.
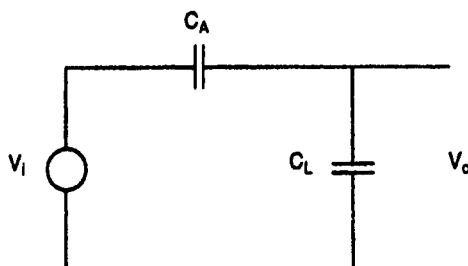
Figure 5. Capacitively Terminated Transmission Line Model of a TEM Horn Antenna

$$V_o = K E \frac{C_A}{C_A + C_L}$$ (2)

where K is the antenna sensitivity and E is the electric field [5]. The low frequency model is also frequency independent if terminated properly.

TEM horns generally maintain constant phase for a wide frequency range. This is because the currents in the conductors travel in the same direction as the fields and stay synchronized to the fields. The only potential problem regarding phase dispersion is the unequal travel paths between the edge currents and center path. A triangular shaped TEM horn, which is longer than it is wide, avoids the varying phase problem.

The guide by Ondrejka provides design equations to determine some important characteristics — the bandwidth and the characteristic impedance. The bandwidth must be as large as possible. The length of the conductors and flare angle of the plates provide the

10

cutoff frequencies. The TEM horn provides a constant impedance where the importance of which has been previously stated . The width and height at the aperture determine the value of impedance. The design equations are presented in Chapter 3.

The TEM horn does not meet the four criteria of an UWB system by itself. Two different models exist for the TEM horn. The low frequency model is frequency dependent until it is capacitively terminated. Ondrejka, et al. [5], also describe a possible solution to the capacitive loading. They add parallel plate extensions to the end of the TEM horn as shown in Figure 6. The extensions change the transmission line model slightly as shown in Figure 7.
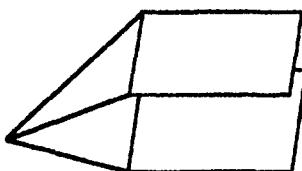

Figure 6. TEM Horn Antenna with
Parallel Plate Extensions
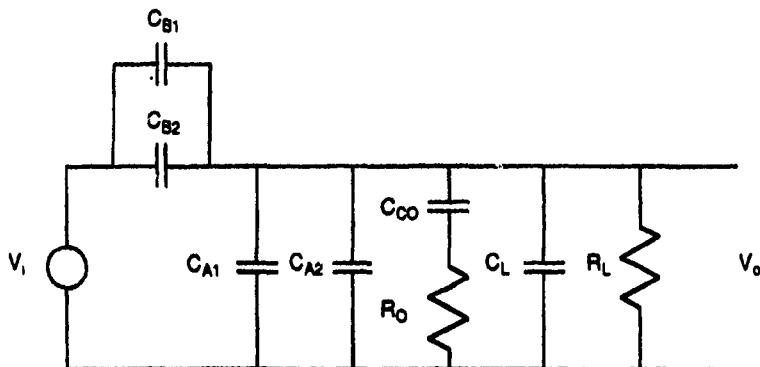
Figure 7. Transmission Line Model of TEM
Horn with Parallel Plate Extensions

11

The coupling between the horn and the fields is represented by C_{B1}. C_{B2} is the shunting capacitance in the horn itself. C_{A1} and C_{A2} are the same quantities for the parallel plates. There is a crossover network composed of C_{CO} and R_O. The values for the capacitors and resistances can be found by [5]

$$C_{A2} = \frac{1}{c\,Z_o}$$
$$C_{A1} = C_{A2} \qquad\qquad (3)$$
$$C_{B1} = \frac{C_{B2}}{2}$$

C_{B2} is the same as C_A from the capacitive model of the TEM horn. The parallel plates enhance the sensitivity of the antenna. As the parallel plate extensions become larger, the low frequency response becomes more like the high frequency response. The optimum performance occurs when the plate area is approximately four times the area of the triangular horn.

The parallel plate extensions do not solve all the shortcomings of a TEM horn. For the TEM horn to provide a gradual transition to free space, the length must be at least half of the longest wavelength. Unfortunately, the parallel plate extensions increase the size even further. In order to maintain the plate area to be four times the horn area, the length of the plates must be twice the length of the horn. At 300 MHz, the horn must be 19.69 inches; thus the plates must be 78.76 inches. By resistively loading along the length of the TEM horn, the length can decrease without adversely affecting the directivity and dispersion [7]. The resistive profile follows the following function:

$$Z(d) = \frac{Z_o}{1 - \frac{d}{L}} \qquad 0 \le d \le L \qquad (4)$$

where L is the total length of the horn. Notice, the impedance tapers from some intrinsic impedance Z_0 at the source end to infinity at the free space end. The taper function is ideal and must be approximated using steps in resistance.

Resistive loading achieves many promising results. It reduces the reflection from the free space end of the TEM horn. Pulse distortion is also minimized. Resistive loading decreases the required length of the horn. For example if Z_0 is chosen to be 14 Ω/m, a

12

14.17 inches horn with resistive loading has a reflection coefficient substantially lower than that of conducting horn 59.06 inches long over the entire range of 100 MHz to 10 GHz [7]. The resistive loading is applied by sputtering copper on polycarbonate substrates ($\varepsilon_R \approx 3$).

Unfortunately, resistive loading has its own problems. The resistive loading dissipates power through its loss mechanism. Maloney [8] provides a good example of this in his dissertation. A perfectly conducting parallel-plate antenna radiates 72% of the incident pulse and reflects 28%. The efficiency, e, is defined as

$$e = \frac{E_{rad}}{E_{rad} + E_{diss}} \tag{5}$$

where E_{rad} is the energy radiated and E_{diss} is the energy dissipated by any loss in the system. Therefore, the efficiency is 100% because perfect conductors do not dissipate any energy. The resistively loaded parallel-plate antenna radiates 10% of the incident pulse and reflects only 2%. However, the efficiency drops to 10% since the loading dissipates 88% of the incident pulse [8]. Since a TEM horn is conceptually an extension of a parallel-plate radiator, a resistively loaded horn exhibits problems similar to those of a resistively loaded parallel-plate radiator. In a low power application, maintaining pulse shape may be more important than efficiency. However, in a high power application, efficiency becomes very important. The thermal heating caused by resistive energy dissipation can become high enough to destroy the antenna.

Tapered Periodic Surfaces

The TPSs developed by Mission Research Corporation [2, 9] overcome many of the shortages of resistive loading. A TPS tapers the size of its elements from one edge to the other. The elements can be of several different geometries: linear, three-legged, four-legged, etc.

There are two basic types of TPS elements — wires and slots; Figure 2 shows a typical wire TPS. Wide strips produce a low impedance and are placed at the conductor end of the TPS. Thin strips give a high impedance which best approximates the free space end. Figure 8 shows a typical slot TPS. Short slots provide a low impedance and are

13

located at the conductor end. Long slots are high impedance structures and match to free space [9].


ground
plane

free
space
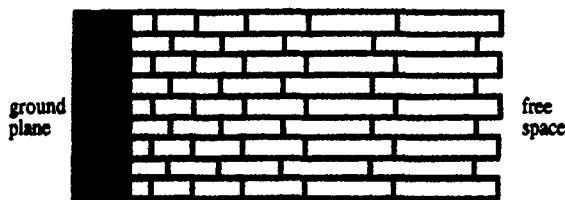
Figure 8. Slot Type of Tapered
Periodic Surface

The actual dimensions of the elements depend on the specific application. The longest element is generally half of the wavelength corresponding to the center of the frequency band of interest. The elements taper to a small fraction of wavelength corresponding to the highest frequency of interest.

Diffraction control is one purpose for a TPS. A TPS reduces reflections much in the same way a resistive loading does. The resistive loading tapers from some Z_0 to an infinite real impedance ($Z=\infty$) at the free space end. A TPS tapers the impedance from some Z_0 to an imaginary impedance ($Z=\pm j\infty$) [2].

A periodic surface of wire elements with very narrow gaps between them is highly reflective over a wide range of frequencies. A highly reflective surface has a sheet impedance very close to 0 Ω/square (like a conductor). As the elements lengths taper towards zero across the surface, the elements are further and further below resonance. The reactance of the surface increases, which decreases the reflection of EM waves. Therefore the impedance gradually transitions from the conductor end to the free space end.

14

Reactive elements do not dissipate power; therefore, a TPS provides an impedance match from a conductor to free space while maintaining a high efficiency. There are many applications for a TPS. RCS test bodies with TPS attachments allow measurements of the object of interest without interference from the edges of the test body. Placing TPS on horn antennas increases the directivity; one unique design places TPS structures around the edges of a box to create an aperture that is frequency independent.

In his thesis, Burleson [10] investigates the use of a TPS to reduce the diffraction from the edge of a ground plane over a wide bandwidth of 2 GHz to 18 GHz. Two different designs are presented — a capacitive taper and an inductive taper. His capacitive taper, shown in Figure 2, is made of two layers of thin strips of conductive material separated by a dielectric slab. His inductive design, shown in Figure 8, consists of skewed thin slots.

Each of Burleson's designs have one edge that presents more of a challenge than the other edge. For his capacitive design, the difficult edge is the ground plane attachment side. The conductor edge requires a low impedance, and therefore, a high capacitance over the entire bandwidth. Ideally the reflection coefficient is unity for this edge. For his inductive design, the free space end is the complicated side. This edge requires a high impedance, or large inductance, over the bandwidth. Ideally, the transmission coefficient is unity for this edge.

The ground plane edge is the most complicated component to design for the capacitive taper. The widest strip that obtains a large reflection coefficient with a gap of 0.005 inches is 0.33 inches. The strip widths then linearly taper from 0.33 inches to 0.005 inches. The center-to-center spacing of 0.335 inches remains constant. The bottom layer is exactly the same but shifted back toward the ground plane edge by half the center-to-center spacing. The dielectric slab between the layers is 0.01 inches thick with a ε_R=4.5 [10].

The free space end is the difficult end to design for the inductive taper. The longest slot that has a high transmission coefficient is 0.35 inches long and 0.005 inches wide. With manufacturing constraints of 0.005 inches, the slot length tapers linearly from 0.005 inches to 0.35 inches. The width of the slots remains constant. The pattern is a skewed

15

array with an offset of 0.0025 inches. The pattern is etched into the same dielectric as in the conductive design.

Testing the designs near grazing incidence simulates the fields of an antenna as shown in Figure 9. The fields are measured with and without the TPS to check the effects of the TPS. Reflection and transmission coefficients are also calculated. Burleson's capacitive design reduces the fields significantly for angles more than 30° into the shadow region. The reflection coefficient remains within 1 dB of unity for 75% of the bandwidth. His inductive design shows less promising results. The transmission coefficient is close to unity for only 25% of the bandwidth. The fields decrease at angles 15° to 30° into the shadow region, but at other angles the reduction is negligible.
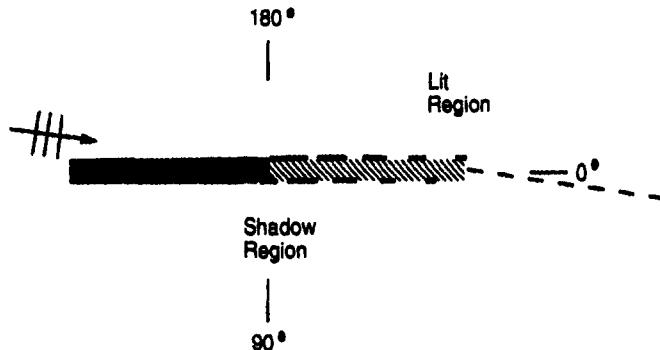

Figure 9. Side View of Test Procedure Used by
Burleson for the Capacitive Taper Design [10]

Burleson provides several suggestions for improvements to the work he started. One idea is to design the TPS such that a specific impedance function is achieved. His design tapers the physical size of the elements. The impedance of the structure is then calculated. Future work is to taper design the elements such that the impedance follows a desired function.

Another suggestion is to design the TPS and then apply it to an antenna or radome. Burleson's research investigates the response of the TPS when illuminated slightly off

16

grazing incidence. However, to test the effects of a TPS when attached to a TEM horn antenna requires actual grazing incidence. Mounting the TPS on the horn is the easiest method to test grazing incidence of the fields.

Summary

This chapter provided a brief description of the background for this thesis. The design criteria of an UWB system were listed. The characteristics of a TEM horn showed that a TEM horn meets many of the criteria. Others have tried many solutions to fix some of the horn's limitations. The theory and application of a TPS was offered as a solution to the deficiencies of a TEM horn.

17

Chapter 3: Methodology

This chapter details the design, model, and test procedures followed in this thesis. There are five main sections in this chapter. The first section describes the design and modeling of a TEM horn antenna. The design is broken down into the three phases that obtain the most important aspects of a TEM horn — low frequency cutoff, high frequency cutoff, and characteristic impedance. The second section details the design of the TPS. The design process is separated into the major components of the design: the TPS elements, the PMM modeling, the sheet impedances, the desired impedance function, and the approximate impedance function. The third section presents the modeling procedure of the TPS. The fourth section describes the manufacturing process and limitations. The final section presents the testing methodology, theory and setup.

TEM Horn Design

In general the design of a TEM horn antenna requires selecting the length of the conductors, the width at the aperture, and the flare angle between the plates. These parameters are adjusted to meet the design criteria of an UWB system.

There are three main aspects to the design of a TEM horn — the low frequency cutoff, the high frequency cutoff, and the characteristic impedance of the horn. The cutoff frequencies determine the limits of the horn's performance. The characteristic impedance provides the details necessary to designing the feed to the antenna.

Low Frequency Design

The low frequency cutoff determines the low end performance of any antenna. Any frequencies lower than the low frequency cutoff do not propagate in the TEM horn antenna. The length of the conductors determines the lowest frequency that propagates in a TEM horn antenna.

18

Two references [5,6] give guidelines for selecting an appropriate length. These guidelines are not considered strict because a TPS will be added to length. Since a TPS appears to be different physical lengths at each frequency, the length of the conductive TEM horn elements are chosen to satisfy the requirements. The additional length of the TPS only enhances the performance of the TEM horn allowing lower frequencies to propagate.

The most restrictive design equation is that which determines the appropriate length based on the interference between the original pulse and the pulse reflected from the end the horn. The equation for the low frequency cutoff is [5]:

$$f_{low} = \frac{c}{4\pi L} \qquad (6)$$

where f_{low} is the low frequency cutoff, c is the speed of light, and L is the length of the TEM horn conductor. Since the lowest frequency of interest is 300 MHz, the length must be at least 3.13 inches.

Another design equation determines the length based on the traveling wave nature of the antenna. The low frequency cutoff (6 dB) equation is [7]:

$$f_{low} = \frac{c}{2L}. \qquad (7)$$

Therefore, the length must be at least 19.69 inches to propagate a signal with 300 MHz components.

Since the two equations provide different solutions the length of the TEM horn, the larger length is chosen so as to satisfy both equations. The actual length is even larger when the TPS is added to the ends; the low frequency cutoff then decreases

High Frequency Design

The high frequency cutoff determines the upper end performance of any antenna. Any frequencies larger than the high frequency cutoff do not propagate in the TEM mode.

19

The flare angle between the plates of the TEM horn determines the highest frequency that propagates in a TEM horn antenna.

The high frequency cutoff is determined by the flare angle between the plates, and consequently, the height of the TEM horn at the aperture. The design equation comes from analysis of a pulse traveling in a TEM horn [5]. The pulse duration, T, is
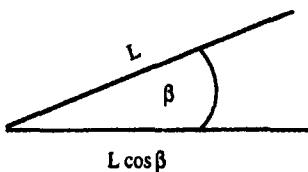
$$T = \frac{L}{c} - \frac{L}{c}\cos\beta = \frac{2L}{c}\sin^2\left(\frac{\beta}{2}\right) \qquad (8)$$

Figure 10. Determination of High Frequency Cutoff

determined by the difference between the time it takes the pulse to travel the length of the conductive elements and the time it takes to travel the boresight length of the horn. The flare angle between the plate and ground plane is β as shown in Figure 10. Since the pulse is approximately a square pulse, the spectrum is a $\frac{\sin(fT)}{fT}$. Therefore, the upper cutoff frequency (6 dB) is [5]

$$f_{high} = \frac{.604}{T} = \frac{(.604)c}{2L\sin^2\left(\frac{\beta}{2}\right)}. \qquad (9)$$

The highest desired frequency is 6 GHz. The flare angle between the plate of the TEM horn and ground plane is 20°. The height of the horn at the aperture is 6.732 inches.

Characteristic Impedance Design

The characteristic impedance is an important design aspect to the TEM horn antenna. The impedance match between the feed and antenna determines the strength of reflections from the feed end of the horn. The gain of a TEM horn is affected by the

20

strength of these secondary reflections. As the reflections decrease, more energy radiates
in the desired direction thus increasing gain. Therefore, choosing a good impedance match
helps reduce the off-boresight field strength.

The height and width of the TEM horn at the aperture defines the characteristic
impedance of the TEM horn. Ideally, the impedance of a broadband antenna is constant. A
constant impedance prevents the reflections and resonances that increase the off-boresight
fields. A TEM horn is nothing more than a transmission line with an impedance that varies
with the width-to-height ratio. The TEM horn keeps the impedance constant by increasing
the width as the height increases. For a TEM horn mounted above a ground plane, the
impedance is [5]

$$
Z_{char} = \begin{cases} \dfrac{2}{\sqrt{K}}(59.95)\ln\left(\dfrac{8h}{w}+\dfrac{w}{4h}\right) & 0\le\dfrac{w}{h}\le 1 \\[3mm] \dfrac{2}{\sqrt{K}}(376.69)\left[\dfrac{w}{h}+2.42-\dfrac{.44h}{w}+\left(1-\dfrac{h}{w}\right)^{6}\right]^{-1} & 1<\dfrac{w}{h}<10 \end{cases} \tag{10}
$$

where K is the antenna sensitivity, w is the width of the horn at the aperture, and h is the
height above the ground plane.

Unfortunately, the characteristic impedance is not the only parameter defined by the
height and width. As the previous section demonstrates, the height also determines the
high frequency cutoff. The height has already been determined to be 6.732 inches.

Phase requirements also constrain the width. The length down the center of the
conductor is different from the length down the edge of the conductor. Thus, the radiated
field is not truly a plane wave. As the width at the aperture decreases, the phase difference
decreases. The phase difference can be found by

$$
\varphi = \frac{\pi w^2}{4\lambda L} \tag{11}
$$

The phase difference is more of a problem at the highest frequency of interest, 6 GHz. In
order to keep the phase difference less than 30°, the width must be less than 5.078 inches.

21

A width of 4.921 inches is chosen. The corresponding characteristic impedance is 288 Ω (assuming the sensitivity, K, is unity).

As with the length, the width at the aperture is larger once the TPS is added; this disturbs the phase difference adversely, but the match to the feed improves. The assumptions of two-dimensional models and local periodicity become questionable if the width is made much smaller.

TEM Horn Modeling

The TEM horn design is modeled using a FDTD electromagnetic code written by Leubbers [12] which utilizes a parallelepiped array in which the TEM horn is modeled. Unfortunately, the geometry of a TEM horn lends itself to one of the weaknesses of the FDTD code — stair stepping error. Since the TEM horn is two triangular plates flared with respect to each other, there are no elements which are orthogonal to each other. Therefore, a stair step of orthogonal elements approximates the geometry of the TEM horn which leads to error in the model.

Selecting a large number of elements to approximate the angled components minimizes the stair stepping error. To minimize the stair step error, the cell size must be as small as possible with respect to the highest frequency. Unfortunately, the size of this model only allows a cell size of 0.197 inches. At 3 GHz, the cell size is $\lambda/20$, the largest cell size at which the approximation does not fail. The model, therefore, is only valid for frequencies less than 3 GHz.

Since a TEM horn is two triangular plates flared with respect to each other, an orthogonal fit must be made for both. The flare angle is fit to a 20° elevation angle. The sequence is shown in Figure 11.

22
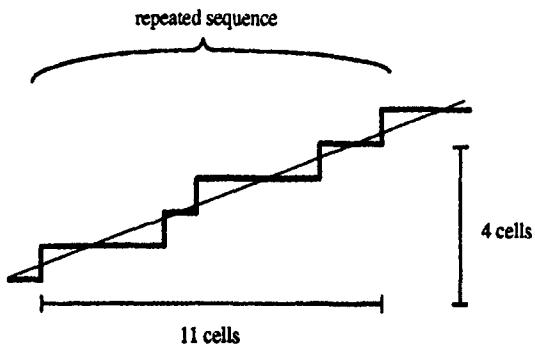
Figure 11. Side View of FDTD TEM Horn
Antenna Approximation

The sequence shown above is repeated nine times for a total length of 100 cells and height of 36 cells. The elevation angle actually produced by the model is 19.8°. The triangular plate must also be approximated by orthogonal elements as shown in Figure 12.
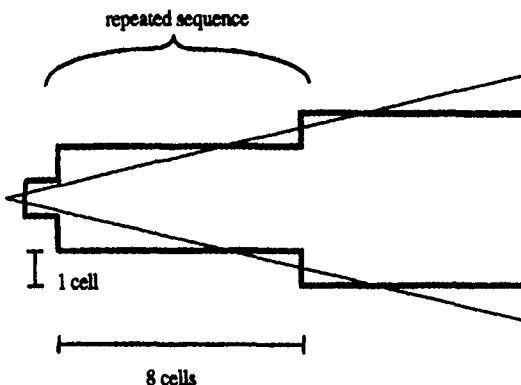

Figure 12. Top View of FDTD TEM Horn
Antenna Approximation

23

The above sequence is repeated 12.375 times for a total length of 100 cells and a width of 27 cells.

In order for the model to produce accurate results, the source pulse must contain frequency components less than 3 GHz. Since the pulse is Gaussian, the width is chosen to be 3 nsec as shown in Figure 13; the pulse spectrum is shown in Figure 14.
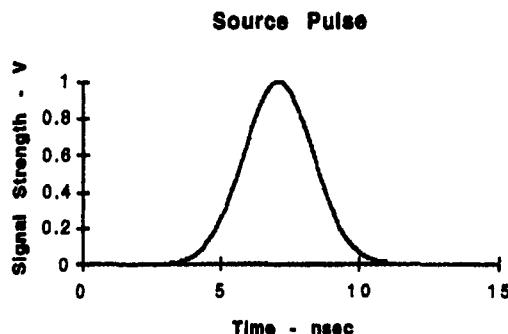
Source Pulse

Figure 13. Source Pulse for FDTD Model
of TEM Horn
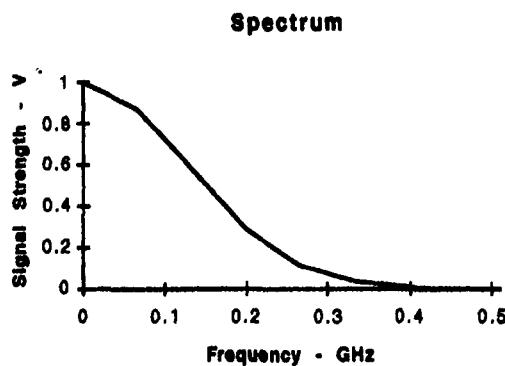
Spectrum

Figure 14. Spectrum of Source Pulse
for FDTD Model of TEM Horn

24

TPS Design

The design of a TPS entails deciding the elements, the element orientation, and the spacing between the elements. The goal is to design a surface with varying sheet impedance that gradually transitions from a very low impedance (like a conductor) to a very high impedance (like free space). A PMM code determines the reflection coefficient of the TPS elements. A transmission line model calculates the sheet impedance of the elements. The actual sheet impedance is fit to a desired sheet impedance.

Element Geometry

Choosing the type of element is the first step in the design of a tapered periodic surface. The type of element determines many important features of the TPS. A TPS in which the elements are arranged along the direction of the taper works best for fields polarized parallel to the edge. Likewise, a TPS with elements oriented in the direction orthogonal to the direction of the taper works best for fields polarized orthogonal to the edge. Elements with three or four legs are polarization insensitive.

There are two main reasons for the choice of orthogonal strips. Previous work shows they are effective in controlling diffraction for electric fields orthogonal to the surface [10]. They are modeled easily in two dimensions. Three-dimensional analysis of the designs requires more computational memory and time than is available.

In his thesis, Burleson [10] shows that layers of conductive strips with a dielectric substrate between are capacitive in nature. As the amount of overlap in the strips decreases, the capacitance decreases. As the capacitance decreases, the impedance approaches $-j\infty$. Therefore, the basic geometrical layout is to have layers of conductive strips separated by a dielectric substrate which overlap in decreasing amounts.

PMM Modeling and Design

The TPSs are designed using a PMM code by Henderson [4]. This code analyzes "multiple infinitely periodic, planar arrays of arbitrarily shaped scatterers imbedded in a lossy stratified dielectric medium". A periodic array of identical elements models the scatterers. Since all the elements are the same, only a reference element must be described. Nodes and the segments in between the nodes physically describe the reference element.

25

For example, a series of eight nodes which are connected by seven segments define a strip, as shown in Figure 15.

dz

dz

dx

|| segment
● node
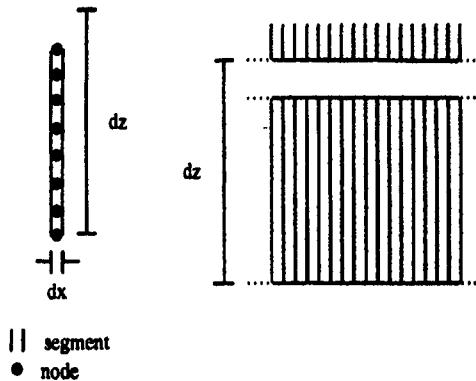
Figure 15. Top View PMM Model
of an Array of Conductive Strips

There is a dielectric substrate of glass epoxy between each layer of conductive strips. The ε_R is approximately 4.5 over the entire bandwidth of 300 MHZ to 6 GHz. Since the difficulty lies in creating a high capacitance (or low impedance), the thickness of the substrate and number of layers depends on achieving a reflection coefficient of unity over the desired bandwidth. Other factors influence the decision. As the number of layers increases, the reflection coefficient becomes closer to unity. However, the time to compute the result grows to unbearable levels. The copper strips are etched onto the top and bottom of each glass epoxy substrate. To combine more than one layer of glass epoxy, the layers must be glued together. This adds another complication to the design. The inherent complications of adding more layers quickly overshadows the gains. Therefore, the geometry of the TPS, as shown in Figure 16, is a double layer. The top layer consists of copper conductive strips separated by increasing gaps. The bottom layer has an identical pattern of conductive strips shifted back by 0.44 inches. A slab of glass epoxy 0.01 inches thick separates the layers.

26
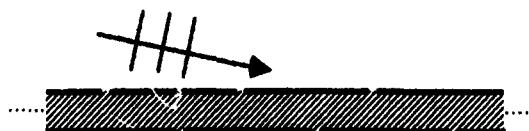
Figure 16. Side View Geometry of
Tapered Periodic Surface

Calculating the field scattered by the model determines the reflection coefficient. One limitation in the PMM code is that true grazing incidence cannot be modeled. The lowest angle from which the incident field can propagate and not violate the assumptions built into the code is 80° off the surface normal. In the actual TEM horn with a TPS attachment the incident field is 90° off the surface normal.

Determining the appropriate strip and gap widths requires several iterations of PMM simulations. Obtaining a large capacitance presents the most difficulty. The first strip and gap combination must have such capacitance. A strip width of 0.87 inches and a gap of 0.01 inches provides a reflection coefficient close to unity for the bandwidth of interest. Now the other TPS elements with lower reflection coefficients are found. The total length, 0.88 inches, is kept constant while the gap width increases in increments of 0.01 inches. This continues until the strips are so small that they no longer maintain capacitive properties. The smallest strip width which maintains capacitive properties is 0.29 inches. When the strip width decreases below 0.29 inches, the taper behaves in an inductive fashion. Therefore, the 59 elements are designed with strips that start 0.87 inches wide (gap width of 0.01 inches) and decrease in steps of 0.01 inches down to 0.29 inches wide (a gap 0.59 inches wide). From this pool of 59 elements, twenty-five elements are chosen to approximate specific impedance functions.

The assumption of local periodicity becomes significant in at this stage of the design. PMM models only one size strip and gap at a time. PMM calculates the reflection coefficient as a function of frequency for this one strip only. To determine the reflection

27

coefficient for a larger gap (and consequently smaller strip) another simulation must be done. To determine the reflection coefficient for the taper, an assumption of local periodicity must be made. The assumption states that at a specific frequency each strip and corresponding gap has a different reflection coefficient. The reflection coefficient decreases along the length of the taper which is consistent with the design goals. The assumption of local periodicity is valid because the gap widths change by only 0.01 inches each time.

Sheet Impedance

In the previous section, PMM calculates the reflection coefficient of the 59 elements. Using the transmission line model shown in Figure 17, the sheet impedance of each element is determined.

$$R = \frac{(Z_s|Z_c) - Z_c}{(Z_s|Z_c) + Z_c}$$
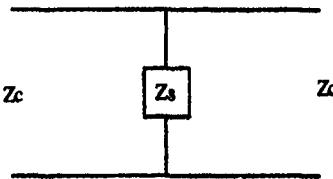
$$Z_s = \frac{-Z_c(1+R)}{2R} \quad \text{where } Z_c = Z_0 \cos\eta$$

(12)

Figure 17. Transmission Line Model of Sheet Impedance
and Equations to Determine the Sheet Impedance
from the Reflection Coefficient

The sheet impedance, Z_S, depends on the reflection coefficient, R, and the angle of incidence, η. The angle of incidence in the simulations is 80°. Note that this model is valid only for fields orthogonal to the taper. A short FORTRAN program converts the

28

reflection coefficient as a function of frequency to impedance as a function of impedance for each element (see Appendix B).

In order to fit the elements impedance to a desired impedance function a meaningful relationship between the impedance and changing parameters must be determined. Figure 18 shows the impedance versus gap width. The impedance as a function of strip width also provides a relationship between the impedance and tapering parameter. Since the impedance is a function of frequency, the impedance as a function of gap width is valid at only one frequency. The design frequency for the impedance function is 3 GHz since it is close to the middle of the frequency band of interest (300 MHz to 6 GHz).

Taper Impedance at 3 GHz
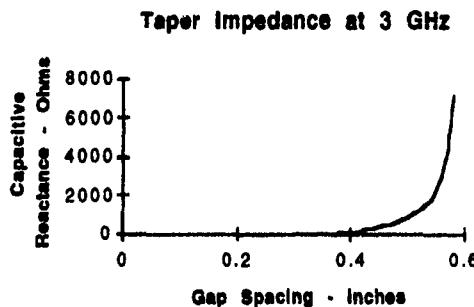
Figure 18. Impedance of Taper Elements as
a Function of the Gap Width at 3 GHz

Desired Impedance Function

There are many methods of achieving impedance matching. One broadband approach is a transmission line which starts at a specific impedance and gradually tapers to another impedance [11]. There are an infinite number of taper functions that fit this description, but a few provide better results than others.

A first logical place to begin is with a function that tapers from a initial Z_1 to Z_n in a linear fashion. The lowest impedance of the taper elements is 0.114 Ω. The largest impedance of the taper elements is 7158.699 Ω. Twenty-five elements provides a smooth

29

enough transition from $Z_1=0.114\,\Omega$ to $Z_{25}=7158.699\,\Omega$. The desired linear impedance taper function is

$$Z_{lin}(d) = 7000d \quad \text{where} \quad 0 \leq d \leq 1 \tag{13}$$

where d is the distance along the length of the taper surface.

Another taper function fits a quadratic curve. Again the function tapers from $Z_1=0.114\,\Omega$ to $Z_{25}=7158.699\,\Omega$. The desired quadratic impedance taper function is

$$Z_{quad}(d) = 7000d^2 \quad \text{where} \quad 0 \leq d \leq 1. \tag{14}$$

Pozar [11] presents other impedance functions that minimize the reflection coefficient of the taper. One such function provides an exponential taper function.

$$Z_{exp}(d) = Z_o e^{d \ln(7000/Z_o)} \quad \text{where} \quad 0 \leq d \leq 1 \tag{15}$$

where Z_0 is the characteristic impedance of free space (377 Ω).

The triangular taper is another impedance taper function. The triangular taper function provides a low reflection coefficient over a wider bandwidth than the exponential taper function. The exponential function gives a lower reflection coefficient, but its bandwidth is not as wide. The triangular function has a deceiving name. The impedance is not triangular; the spatial derivative of the natural log of the normalized impedance is triangular. Therefore, the triangular impedance taper function is

$$Z_{tri}(d) = \begin{cases} Z_o e^{2d^2 \ln(7000/Z_o)} & \text{for } 0 \leq d \leq \frac{1}{2} \\ Z_o e^{(4d-2d^2-1)\ln(7000/Z_o)} & \text{for } \frac{1}{2} \leq d \leq 1 \end{cases} \tag{16}$$

Four taper functions are designed and simulated. The two that perform the best are built and tested. Figure 19 shows the four desired taper functions as a function of length.

Desired Sheet Impedances
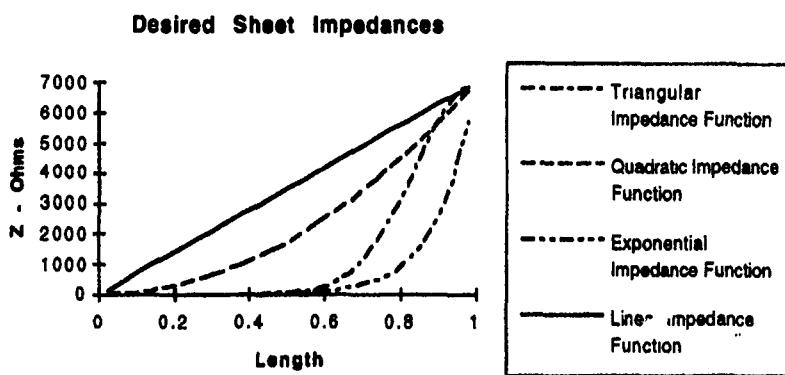
Figure 19. Desired Impedance Taper
Functions at 3 GHz

Approximated Impedance Function

The desired impedance taper functions are functions of length (see Figure 19). The taper impedances are functions of gap width (see Figure 18). Matching the impedances determines the gap width as a function of length. Building a taper from the gap width versus length function provides an approximate impedance function. The approximate taper function fits 25 impedance points to the desired taper function using a smallest difference method. Figures 20 through 23 depict how well the approximate function fits the desired function.

31

Triangular Sheet Impedance
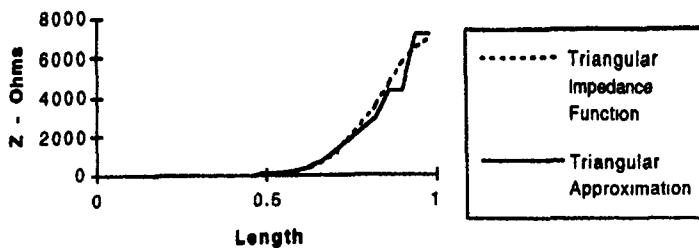
Figure 20. Approximate versus Desired Triangular
Sheet Impedance Function at 3 GHz

Linear Sheet Impedance
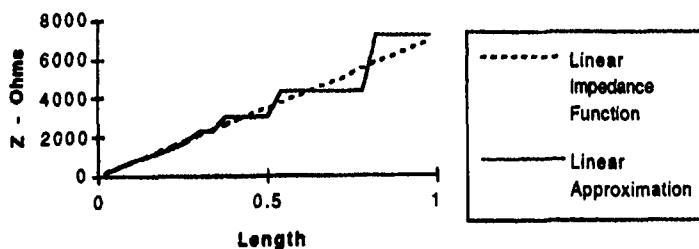
Figure 21. Approximate versus Desired Linear
Sheet Impedance Function at 3 GHz

32

Exponential Sheet Impedance
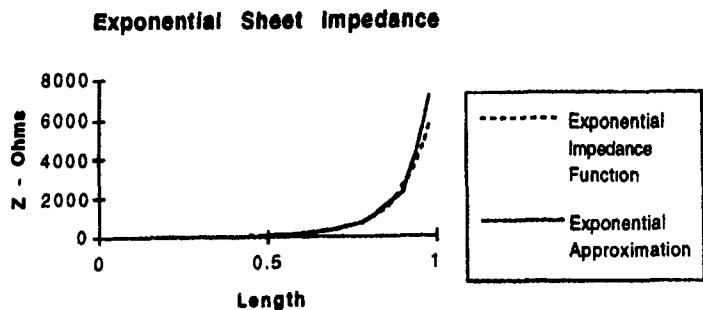
Figure 22. Approximate versus Desired Exponential
Sheet Impedance Function at 3 GHz

Quadratic Sheet Impedance
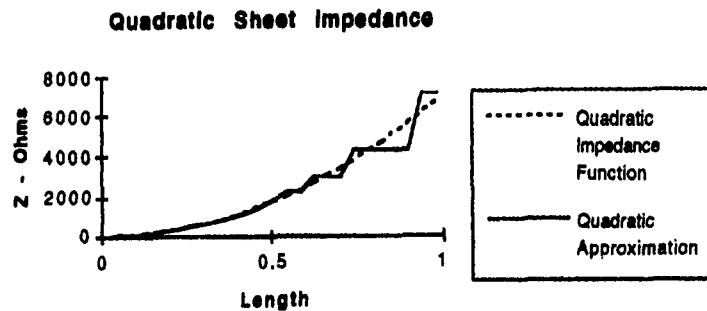
Figure 23. Approximate versus Desired Quadratic
Sheet Impedance Function at 3 GHz

TPS Modeling

A two-dimensional FDTD code written by Leubbers [12] models each TPS. The two-dimensional code is very similar to the three-dimensional code used previously to

33

model the TEM horn. The biggest difference is that the $\hat{z}$ dimension is assumed to be infinite. There are two versions of the two-dimensional code — transverse electric (TE) and transverse magnetic (TM). A TEM horn antenna lends itself to analysis using the TE code because the electric fields are normal to the surface of the TPS

The TE code utilizes a rectilinear grid of x and y components [12]. Only E_x, E_y, and H_z fields are present. A side view in a two-dimensional sense models the TEM horn and TPS most meaningfully. A two-dimensional analysis does not take into account the triangular shape. This eliminates the possibility of obtaining simulation results that correspond directly to test results. However, the simulations demonstrate how well each taper reduces the off-boresight fields.

The performance of the TEM horn and TPS attachments as a radiating antenna is not simulated. The simulations test the ability of the TPS design to reduce the off-boresight fields. The TPS model is shown in Figure 24.

Figure 24. Two-Dimensional FDTD Model of TPS

The model has a metal plate with a dielectric slab attached to the right of the plate. Conductive strips of the TPS are overlaid onto the dielectric substrate in the pattern dictated by the approximate impedance taper function. A Gaussian pulse is placed at the far left under the metal plate. The fields propagate for 20 nsec. A near field to far field transformation [3] computes the far field response at several angles. The angles correspond to on and off boresight points of interest.

The grid space for this model is 4210 by 43 cells. The fields are sampled for 32768 time steps. Six different geometries are simulated — the triangular taper, the exponential taper, the quadratic taper, the linear taper, a short metal plate, and a long metal plate. The

34

short plate is 19.69 inches long and represents the original reference TEM horn. The long plate is 41.69 inches long and represents a TEM horn as long as both the original horn plus the TPS attachment.

Manufacture Specifications

Due to time and financial constraints only three test bodies can be fabricated. The triangular and exponential tapers and the reference TEM horn are manufactured by Mission Research Corporation (MRC). The triangular and exponential taper functions reduce the off-boresight fields better than the linear and quadratic tapers (see Chapter 4).

MRC constructs the tapers with a method similar to printed circuit boards. The exact geometries designed in AutoCAD are presented in Figure 25 and Table 1. CompuRoute Inc. develops a photoetching mask from the AutoCAD files. MRC etches the copper strips into glass epoxy. The single sheet of copper strips with glass epoxy between was mounted to styrofoam ($\epsilon_R \approx 1.1$) with double sided tape. The styrofoam gives the structure the physical support to remain rigid. The actual copper and glass epoxy combination is only 0.01 inches thick.

element number	triangular taper		exponential taper	
	strip width (inches)	gap width (inches)	strip width (inches)	gap width (inches)
1	0.87	0.01	0.86	0.02
2	0.87	0.01	0.86	0.02
3	0.87	0.01	0.84	0.04
4	0.86	0.02	0.83	0.05
5	0.85	0.03	0.80	0.08
6	0.84	0.04	0.77	0.11
7	0.83	0.05	0.64	0.24
8	0.81	0.07	0.62	0.26
9	0.76	0.12	0.60	0.28
10	0.63	0.25	0.52	0.36
11	0.60	0.28	0.51	0.37
12	0.51	0.37	0.51	0.37

35

13	0.50	0.38	0.50	0.38
14	0.48	0.4	0.49	0.39
15	0.46	0.42	0.48	0.40
16	0.43	0.45	0.47	0.41
17	0.39	0.49	0.45	0.43
18	0.36	0.52	0.43	0.45
19	0.34	0.54	0.41	0.47
20	0.33	0.55	0.39	0.49
21	0.32	0.56	0.36	0.52
22	0.31	0.57	0.34	0.54
23	0.31	0.57	0.33	0.55
24	0.30	0.58	0.31	0.57
25	0.30	0.58	0.31	0.57

Table 1. Detailed List of Strip and Gap Widths for Both
the Triangular and Exponential Tapers
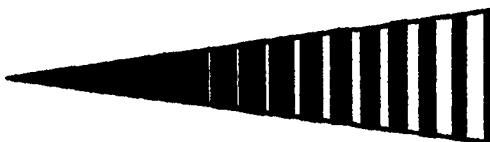
Figure 25. Top View of TEM Horn
Antenna with TPS Attachment

MRC attaches a thin wire at the narrow feed end of the horn. The wire fits into an
SMA connector. The pulse generator connects to the feed point by this SMA connector.

Testing Procedure

The High Energy Research and Technology Facility of USAF Phillips Laboratory
at Kirtland AFB, New Mexico provides the facilities and equipment to test the three test
bodies. The setup consists of a large ground plane, styrofoam supports, test equipment,
and a rotating arm system to track the probe in elevation angle as shown in Figure 26.

36

The test bodies are mounted above the ground plane to act as if both plates of the TEM horn are present. The styrofoam supports elevate the horns to the 20° design angle. The foam supports introduce a small reduction in field levels and shapes. These errors are small, and the need for supports outweighs the costs.

Figure 26. Test Setup showing TEM Horn,
D-dot Probe, and Rotating Arm System

A rotating arm system allows the probe to remain at a constant distance, 44.173 inches, from the horn while rotating in elevation. The probe is at a constant azimuth angle of 0°. The arm system rotates about an axis that runs through the edge of the reference horn. The edge of the reference horn is the edge treated with the TPS. Nine different angles are chosen to test the ability of the system to reduce the off-boresight field levels as a

37

function of elevation angle. The chosen angles are 0° (on boresight), 20°, 30°, 40°, 50°, 60°, 70°, 80°, and 90°. The angles stopped at 90° due to the cable length.

The test equipment consists of a pulse generator, a digital sampling scope, a personal computer, and a probe. The pulse generator fills the role of the source. The pulse generator is a Picosecond Pulse Labs Model 10050 pulse generator. The generator produces pulses of 10 nsec duration at a repetition rate of 100 kHz. The delay is 63 nsec for proper triggering. The pulses have a rise time of approximately 60 psec. The sampling scope is a Tektronics 11801A digital sampling scope. The scope records the response of the horns for later analysis. The scope averages 2048 pulses per trace. This provides a very smooth curve that does not contain spurious data. A personal computer with LabVIEW software provides permanent storage for the traces. LabVIEW records the trace on the display of the scope to an ASCII data file for post-processing.

The probe used to record the response of the test bodies is a D-dot probe. A D-dot probe does not report the exact response; it reports a voltage level based on the time derivative of the response. The probe has two channels which, if the probe is normal to the field, are equal and opposite signals. Unfortunately, a D-dot probe is also sensitive to any tilt angle of the probe with respect to the electric field. Therefore, if the probe is not normal to the electric field, one channel is not equal and opposite to the other. To avoid tilt angle discrepancies only one channel is recorded. Thus, the recorded trace may be a scaled version of the true response. Actually, a D-dot probe produces a signal based on $\partial D(t)/\partial t$. However,

$$D(\omega) = \varepsilon(\omega)E(\omega) \xleftrightarrow{\text{Fourier}} D(t) = \varepsilon(t) \otimes E(t). \tag{17}$$

For free space and air, the permittivity is considered to be constant, ε_0. The convolution in the time domain becomes multiplication by a constant, and

$$D(\omega) = \varepsilon_0 E(\omega) \xleftrightarrow{\text{Fourier}} D(t) = \varepsilon_0 E(t) \tag{18}$$

The pulse generator drives the system with pulses with long pulse width.

Although technically the unit step function exists forever, most systems have an impulse response that lasts only for a relatively short duration of time. If we use a low frequency square-wave generator whose repetition

38

rate is much longer than the duration of the impulse response of the system, the system for all practical purposes sees a step. After recording the step response of the system, one can take the derivative of the output graph as a function of time. This will be the impulse response of the system. [13]

The probe already reports the time derivative of the response. Therefore, the scope trace is actually the impulse response of the system. The scope reports

$$V(t) = A\varepsilon_0 E(t) \tag{19}$$

where A is a factor between zero and unity due to any tilt angle and only one channel. The relative field levels are normalized by the reference horn response at that particular angle thereby canceling the permittivity of free space and the tilt factor due to the probe. The pulser drives the system with an effective step, but the probe reports the impulse response due to its time derivative nature.

Summary

This chapter detailed the design, model, and test processes. There were five main sections in this chapter. The first section described the design and modeling of a TEM horn antenna. The second section detailed the design of the TPS. The third section described the modeling procedure of the TPS. The manufacturing process and limitations were described in the fourth section. The final section presented the testing methodology, theory and setup.

39

Chapter 4: Results and Analysis

The purpose of this chapter is to list the results of the modeling and testing of the TEM horn and TPSs designed in this thesis. The results of many of the models are explained in order to clarify the reasons behind many of the decisions that are made.

There are six sections to this chapter. The first section gives the results of the TEM horn model. The second details the results of the PMM modeling and design. Some examples of the results are provided to give a understanding of the models. The fourth section describes the sheet impedance of the taper elements. The fifth section details the approximate impedance functions at frequencies other than the design frequency. The sixth, and final, section provides the results of the testing phase of this thesis.

TEM Horn Modeling

The FDTD model for the TEM horn confirms the directive behavior of the antenna. The on-boresight field levels are higher than the off-boresight levels.

The approximate nature of the model does not allow a complete estimate of the TEM horn performance. The frequency content of the source pulse is only a fraction of the operating bandwidth of the horn. The stair stepping error prevents use of the full bandwidth. Computing limitations do not allow a better approximation.

PMM Modeling and Design

The PMM models the reflection coefficient for each element separately. The goal is to taper the reflection coefficient from unity to zero along the length of the taper. Since the taper consists of conductive strips separated by a dielectric slab, the taper become less reflective as the gap width between the strips increases.

The most difficult edge to design is the conductor edge. The goal is to find a gap width which produces a reflection coefficient close to unity over as much bandwidth as

40

possible. Figure 27 shows the magnitude of the reflection coefficient for the first element of the taper. The strip width of the first element is 0.87 inches. The gap width is 0.01 inches.

Reflection Coefficient Magnitude
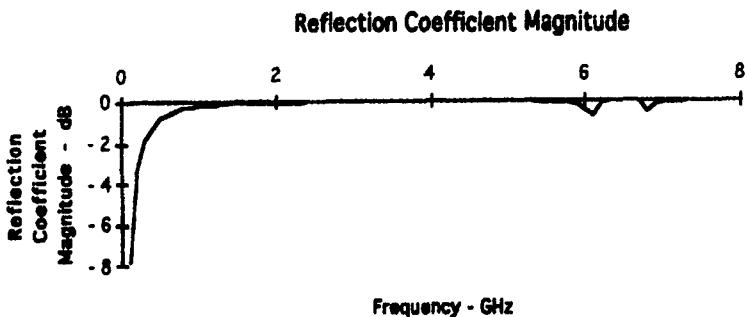
Figure 27. Reflection Coefficient Magnitude
for the First TPS element

Reflection Coefficient Phase
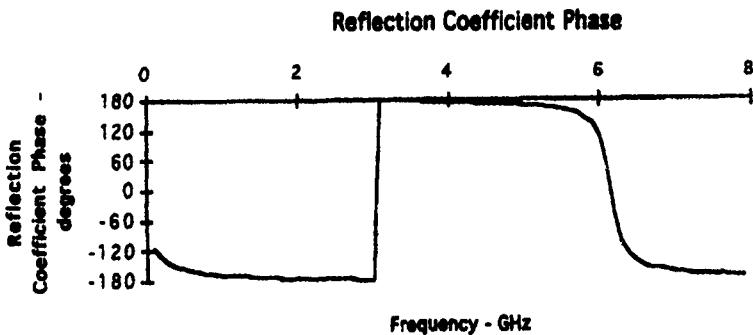
Figure 28. Reflection Coefficient Phase
for the First TPS Element

41

The magnitude of the reflection coefficient is close to unity except at low frequencies. However, the reflection coefficient is less than 2 dB at 300 MHz. Therefore, the first element allows large amounts of reflection at the low frequencies. This large reflection coefficient provides a low impedance.

The phase plot of the reflection coefficient for the first TPS element shows good results in Figure 28. The phase function is fairly linear from 300 MHz to 5.8 GHz. There is some dispersion at the higher frequencies also, but it is difficult to detect.

Figure 29 shows the reflection coefficient magnitude for the tenth TPS element. The tenth element strips width is 0.78 inches. The corresponding gap is 0.1 inches wide. Notice the lower frequencies are less reflective. This causes the impedance to increase. Figure 30 shows the phase response of the tenth TPS element. At high frequencies the response becomes more linear. At low frequencies the phase linearity suffers and a small amount of dispersion occurs.

Reflection Coefficient Magnitude
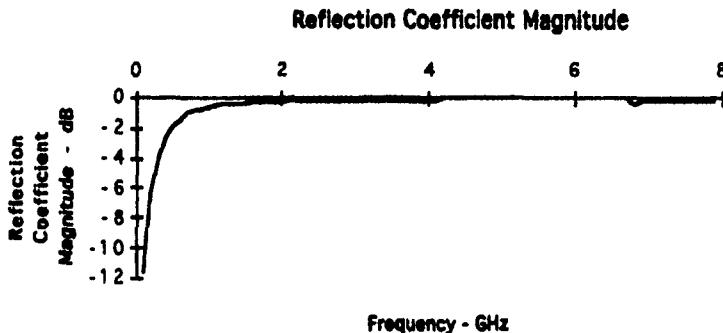
Figure 29. Reflection Coefficient Magnitude
for the Tenth TPS Element

42

Reflection Coefficient Phase
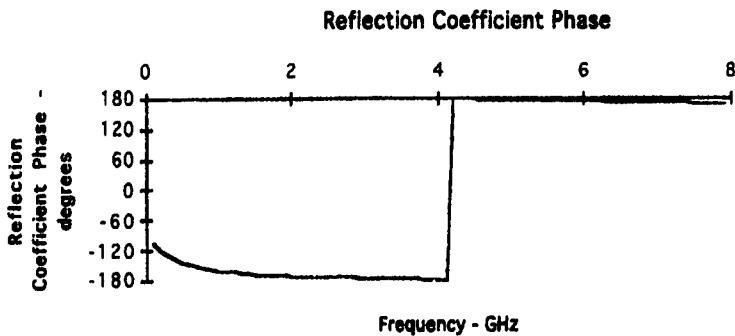
Figure 30. Reflection Coefficient Phase
for the Tenth TPS Element

The above plots show the reflection coefficient decreasing as the gap grows. This trend continues until the gap geometry begins to dominate. When the gaps define the electrical properties of the TPS, the taper becomes inductive. Babinet's principle explains the change in electrical properties. The fifty-ninth element is the last element at which the strip width dominates the electrical behavior of the TPS. The strip width for the last element is 0.29 inches; the gap width is 0.59 inches. The reflection coefficient magnitude is shown in Figure 31. The phase is shown in Figure 32.

43

Reflection Coefficient Magnitude
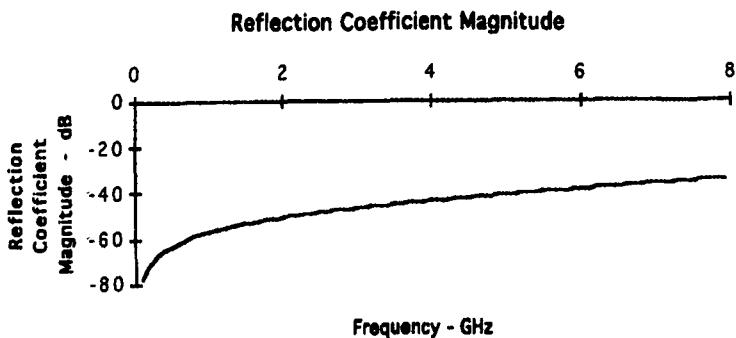
Figure 31. Reflection Coefficient Magnitude
for the 59th TPS Element

Reflection Coefficient Phase
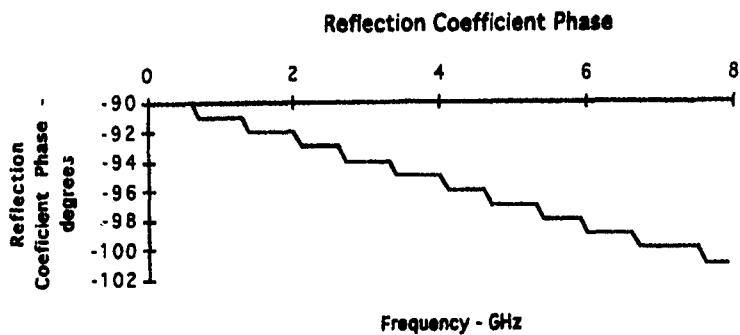
Figure 32. Reflection Coefficient Phase
for the 59th TPS Element

The reflection coefficient is low throughout the entire bandwidth. Low reflection coefficient is the goal for the free space end of the taper. Likewise the phase response of

44

the reflection coefficient is linear. There is no appreciable dispersion from the last element of the taper.

These few examples of the PMM modeling show the design process and results used to determine the taper function. Elimination of the dispersion that distorts the pulse requires a linear phase response throughout the taper. This is not achieved which is evident in the test results. The reflection coefficient is to taper from unity to zero along the length of the taper. This is achieved reasonably well.

Sheet Impedance

After calculating the reflection coefficients for each of the elements, the elements are pieced together to form the pool of elements from which the impedance functions will be approximated. The reflection coefficient changes with different gap widths. Again, the goal is to taper the reflection coefficient magnitude from unity to zero as the gap width increases while maintaining a linear phase response.

Appendix A shows the reflection coefficient's magnitude and phase versus gap width for the 300 MHz, 1 GHz, 3 GHz, and 6 GHz. Figures 33 and 34 show the reflection coefficient at the design frequency of 3 GHz.

Reflection Coefficient Magnitude
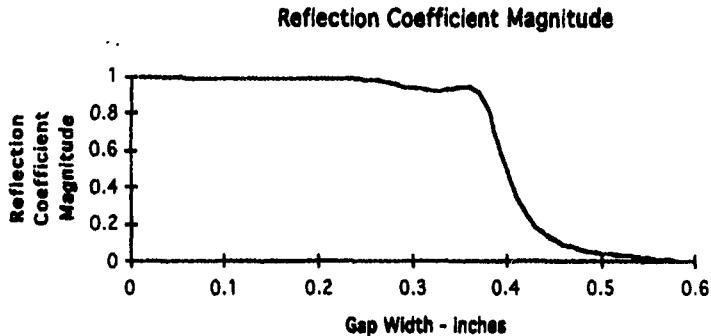
Figure 33. Reflection Coefficient Magnitude versus
Gap Width of the TPS elements at 3 GHz

45

ADA289708

Reflection Coefficient Phase
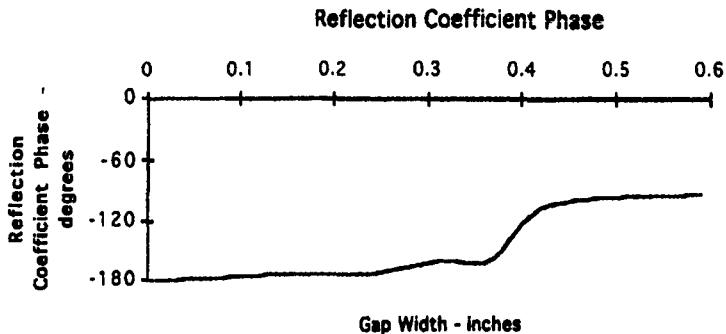
Figure 34. Reflection Coefficient Phase versus
Gap Width of the TPS elements at 3 GHz

The magnitude does taper from unity at the conductor edge to zero at the free
space edge. The reflection coefficient experiences the greatest change between 60% and
80% of the length. When approximating the desired impedance functions, the elements
in the 60% to 80% region perform the curve fit. The phase response is fairly linear.

Approximate Impedance Functions

In Chapter 3, the several plots demonstrate the relationship between the desired
impedance functions and the approximate impedance functions of the tapers. The curve
fits show for each of the four taper functions at the design frequency of 3 GHz.

The impedance functions at other frequencies do not have the same fit to the
desired functions. In fact, the approximate impedance functions at other frequencies
often have very different curves.

Figure 35 shows the approximate impedance function at 300 MHz, 1 GHz, and 6
GHz compared to the desired triangular impedance function. Figure 36 shows the
approximations to the linear impedance function. The exponential approximations are in
Figure 37. Figure 38 gives the approximations to the quadratic impedance function.

46

Triangular Sheet Impedance Approximations
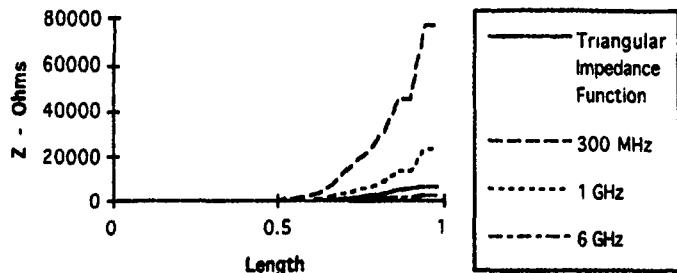
Figure 35. Approximate Impedance Functions
at 300 MHz, 1 GHz, and 6 GHz

At low frequencies, the approximate impedance function does not fit a triangular function. As the frequency increases, the function approximates the triangular function more closely. This trend continues for all the taper functions.

Linear Sheet Impedance Approximations
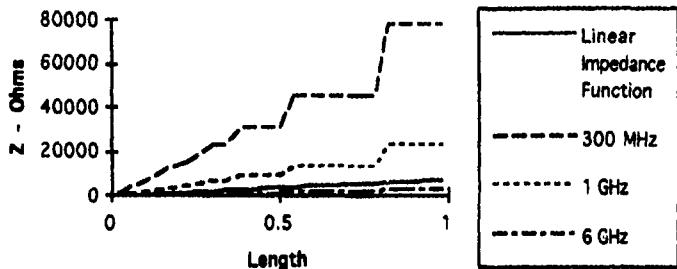
Figure 36. Approximate Linear Impedance
Functions at 300 MHz, 1 GHz, and 6 GHz

47

ADA289708

The linear approximations do not follow the desired linear impedance function.
They approximate other linear functions.

Exponential Sheet Impedance Approximations
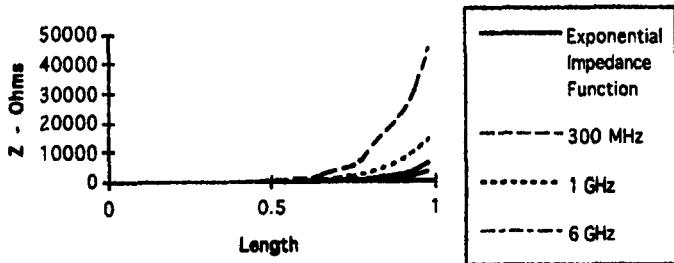
Figure 37. Approximate Exponential Impedance
Functions at 300 MHz, 1 GHz, and 6 GHz

The exponential approximations fit the desired function more closely than the
triangular, linear, or quadratic approximations. Like the linear function, the
approximations at the other frequencies follow other exponential functions.

Quadratic Sheet Impedance Approximations
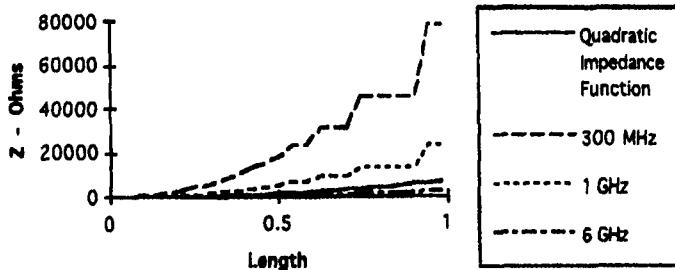
Figure 38. Approximate Quadratic Impedance
Functions at 300 MHz, 1 GHz, and 6 GHz

48

The quadratic approximations uphold the trends seen in the other taper approximations. The approximations at other frequencies follow different quadratic functions. As the frequency increases, the approximation fits the desired function more closely.

The fact that the impedance approximations do not meet the desired functions is not surprising. Impedance is typically a function of frequency. All the tapers gradually increase the impedance along the length of the TPS at all frequencies of interest. Therefore, all the tapers provide a better match to free space than the TEM horn alone.

TPS Modeling

FDTD models the tapers to determine which taper reduces the off-boresight field levels the most. Computer limitations prevent full three-dimensional modeling of the tapers. Therefore, the radiation performance can not be evaluated. Instead a two-dimensional scattering performance is investigated.

A scattering evaluation does not allow direct comparison between the model and the test. A scattering evaluation, however, provides a method for determining which tapers reduce the edge diffraction the most. A source excites a Gaussian pulse at the metal edge of the taper. The field levels are calculated for 32768 time steps to allow the response to reach steady state. A near field to far field transformation allows the far zone response to be evaluated [3].

Figure 39 shows the geometry used to determine the scattered field of the tapers for four angles—0°, 30°, 60°, and 90°. The angles are rotated 20° to correspond to the angles in the elevated upper plate of the TEM horn.

49
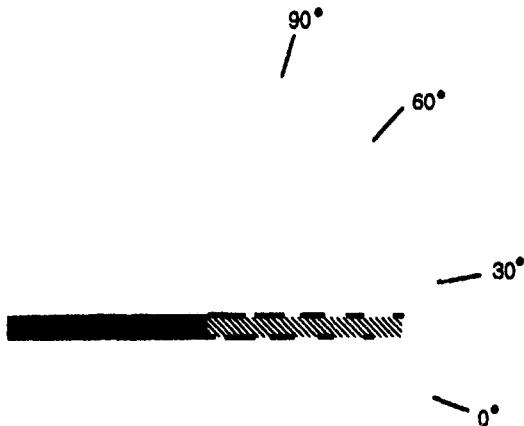
Figure 39. FDTD Model Geometry and
Test Angle Locations

There are nine test angles. Only four test angles are shown for demonstration.
The other results are in Appendix C.

Figure 40 shows the scattered fields for the reference plate. The plate is 19.69
inches long and represents the reference TEM horn. The first pulse is the energy
scattered from the back end of the plate. Since all the tapers begin with a metal plate, the
first pulse is present in all the simulations. Adding the different tapers does affect the
fields scattered from the back edge.

50
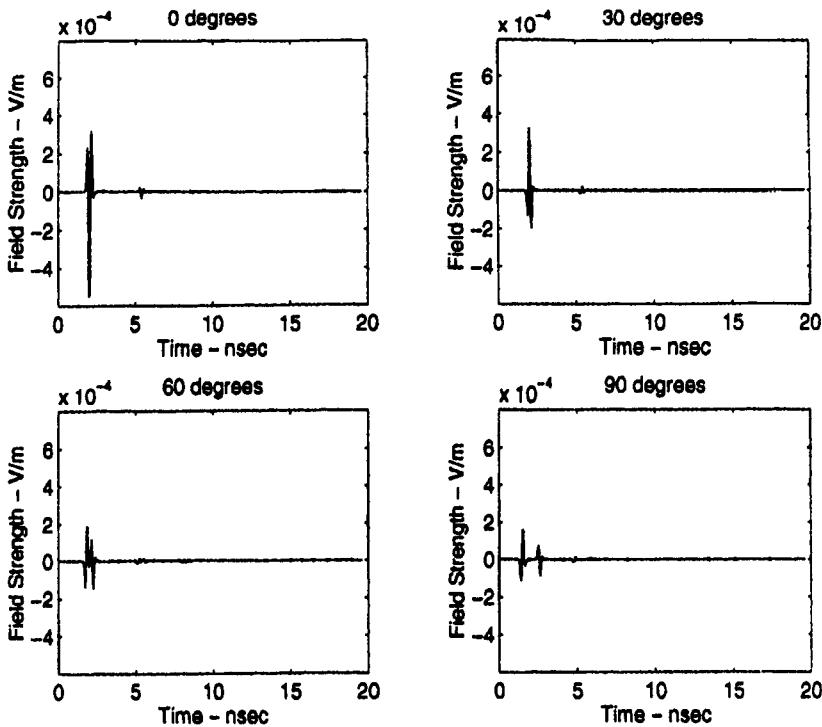
Figure 40. Scattered Field Plots from the
Reference Plate at 0°, 30°, 60°, and 90°

The field diffracted from the front edge partially overlaps with the field diffracted
from the back edge. As the angle becomes greater the two responses separate due to the
increasing travel distances. The responses due to multiple reflections occur
approximately 3.33 nsec later.

The field levels decrease as the angle increases. This is because the diffraction
decreases as the sample locations become more orthogonal to the plate. The 0° test
location actually sees the source pulse. The 30° location has lower field levels than the

51

field levels at 40° location. This is due to the 30° sample point's proximity to grazing incidence.

The response of the triangular impedance taper is shown in Figure 41. The taper reduces the diffracted field levels for angles 60° and greater. The performance continues to improve as the fields are sampled at greater angles. The triangular taper reduces the diffracted fields better than the other tapers on the boresight.
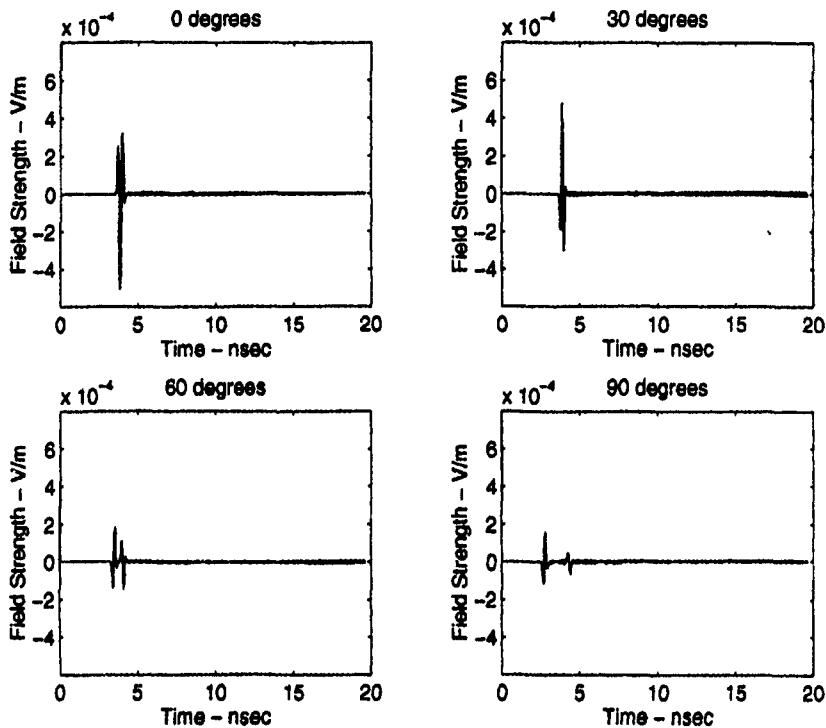
Figure 41. Scattered Field Plots from the
Triangular Taper at 0°, 30°, 60°, and 90°

52
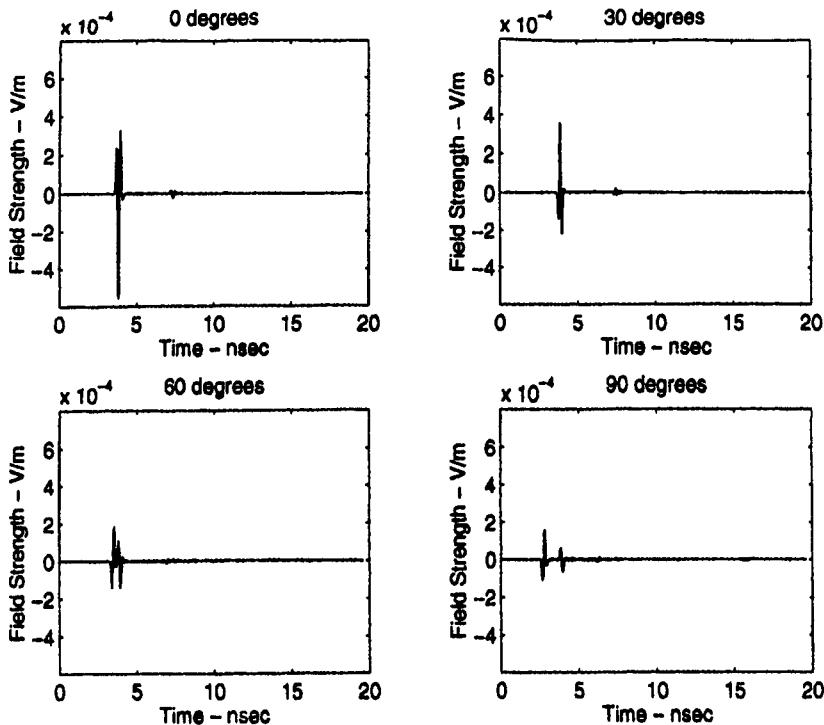
Figure 42. Scattered Field Plots from the
Quadratic Taper at 0°, 30°, 60°, and 90°

Figure 42 shows the diffracted fields from the quadratic taper. The quadratic
taper performs similarly to the triangular taper. Of the four tapers, the quadratic taper's
performance is average. The performance improves as the angle increases. The
quadratic taper reduces the field at the lower angles more than the triangular taper. The
triangular taper reduces the field level better at large angles. For example at the 30° test
location, the field diffracted from the edge of the quadratic taper is 2.74 dB lower than the
field diffracted from the triangular taper. While at the 90° test location, the triangular
taper outperforms the quadratic taper by 1.643 dB.

53
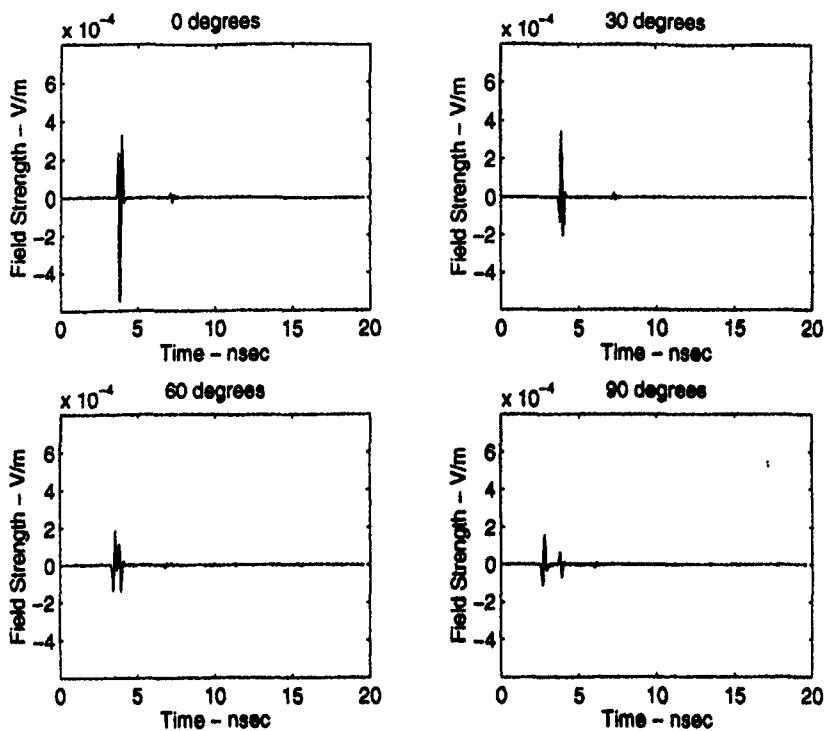
Figure 43. Scattered Field Plots from the
Linear Taper at 0°, 30°, 60°, and 90°

The linear taper's performance is shown in Figure 43. Again the reduction of diffracted fields improves as the test angle increases. However, the linear taper does not reduce the fields as much as the other tapers in most test locations. This becomes more apparent at the 90° test location. The linear taper reduces the diffracted fields by 1.85 dB when compared to the diffracted fields from the reference plate. The triangular taper reduces the relative field level by 4.214 dB.

54
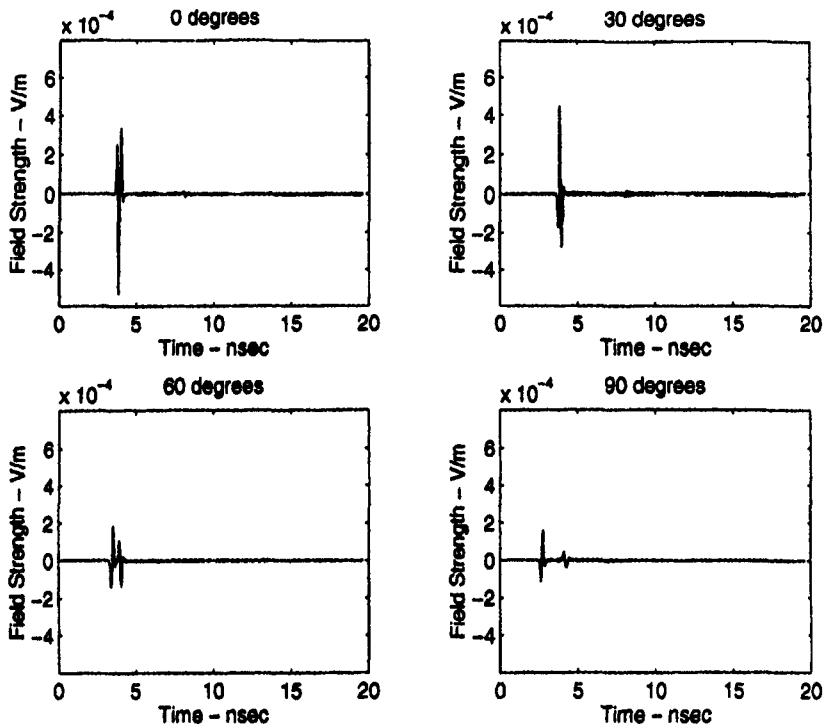
Figure 44. Scattered Field Plots from the
Exponential Taper at 0°, 30°, 60°, and 90°

The exponential taper offers the greatest amount of diffraction control. Figure 44 contains the plots of the response of the exponential taper. The exponential taper reduces the diffracted field levels more at the higher test angles than any of the other tapers. The fields at the 90° location are 3.625 dB lower than the fields from the next best taper, the triangular taper.

55
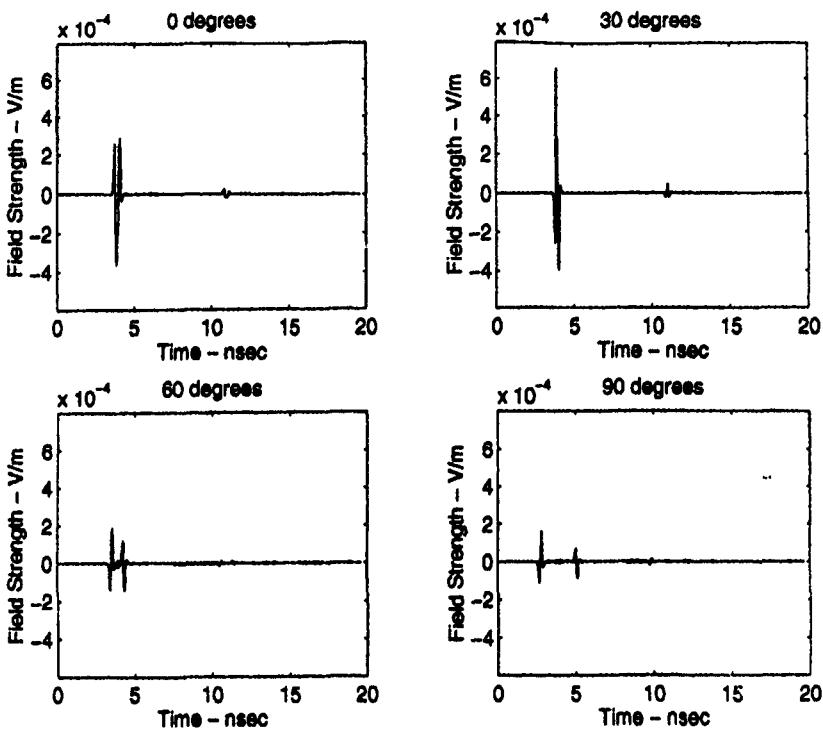
Figure 45. Scattered Field Plots from the
Long Plate at 0°, 30°, 60°, and 90°

A final model checks the possibility of extending the plate length to 41.69 inches.
This is the length of the horns with the TPS attachments. The diffracted field plots are
shown in Figure 45. The longer plate reduces the diffracted fields at the lower angles
better than the tapers. However, the tapers decrease the field levels further off-boresight
than the long plate. The linear taper reduces the fields 1.809 dB lower than the long plate
at the 90° test point. Keep in mind, the linear taper has the worst performance of all the
tapers at this location.

56

Financial and time constraints limited the number of designs to be built and tested. Only two taper designs are chosen. Clearly, the long plate and linear taper offer the least reduction performance for the off-boresight fields. The exponential taper decreases the field levels the most and, therefore, makes a good choice. The triangular and quadratic tapers offer approximately the same level of results. The triangular taper has a lower field level at ⬚   t location than the quadratic taper. This may lead to higher on-boresight field levels since there will be less diffraction from the edge in the 0° direction. Therefore, the exponential and triangular tapers are built and tested.

One important limitation must be highlighted. The models are two-dimensional. The test bodies are three-dimensional. The models can be used only in a qualitative sense to demonstrate which taper functions reduce the diffracted fields the most. The amount of reduction cannot be used as an estimate for actual performance. The reduction levels produced by the models can be used only to rank the performance of the taper functions.

Testing

The tests of the TEM horn with and without the TPS attachments result as expected. The field levels decrease as the fields are sampled at larger angles. This occurs for all the objects tested. Since a horn radiates most of the energy in the on-boresight direction, the field levels decrease as the probe is moved off boresight. The TPS attachments reduce the off-boresight fields even further.

There are three test objects — an all metal reference horn 19.69 inches long, a horn with triangular taper, and a horn with exponential taper. The testing determines which taper reduces the off-boresight electric field levels the most. An all metal horn provides a reference and normalization factor. The impulse response of each horn is recorded at a specific angle. The trace of the impulse response shows the peak level of the field diffracted from the free space edge. Normalizing the peak level of the tapered horns by the reference horn provides a meaningful comparison.

Appendix D contains the trace plots for the two tapered horns and reference horn. A few examples of the trace plots are explained in detail. The plots in Appendix D are similar and can interpreted using similar methods.

57

Figure 46 shows the impulse response of the reference horn on boresight. The time divisions are 100 psec. There are three main pulses. The first pulse is the main radiated pulse. The second pulse is the pulse of interest. It is the energy diffracted by the edge. Notice the diffracted pulse has a polarity opposite of the radiated pulse. The third pulse is the pulse resulting from the diffraction off the edge and reflecting off the ground plane.

On Boresight (0 degrees)
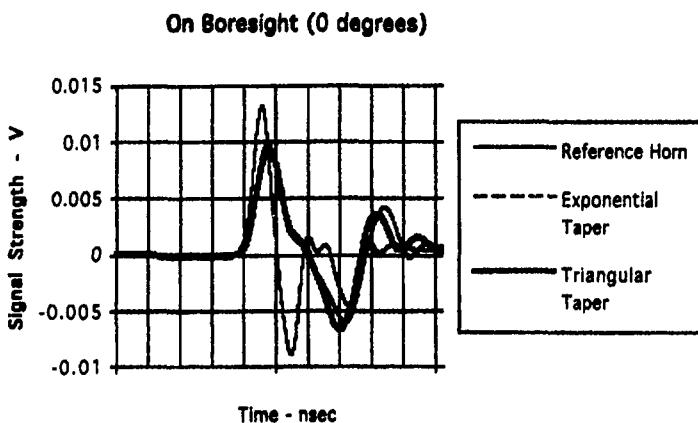
Figure 46. Electric Field Impulse Response at
the On-Boresight for the Reference Horn,
Exponential Taper, and Triangular Taper

Figure 46 also shows the impulse response of the triangular and exponential tapers. The first pulse is the main radiated pulse. The second pulse is the pulse diffracted from the edge, showing the time shift due to the longer length with TPS attachments. The triangular taper is electrically shorter than the exponential taper. The different tapers become transparent to the pulse at slightly different locations.

58

The tapers do reduce the diffracted field levels. As predicted, the exponential taper performs better than the triangular taper. The triangular taper optimizes bandwidth which degrades performance.

One disturbing result is the reduced main radiated pulse shown in Figure 46. One of the goals was to maximize the on-boresight field levels. The tapers distort the main pulse and the pulse broadens. The spreading of the pulse forces the peak level to decrease. The tapers do not have a true linear phase response. The phase dispersion causes some time delay and spreads the pulse. The additional length of the TPS decreases the high frequency cutoff. The high frequencies cannot propagate and the pulse becomes wider.

The off-boresight impulse response at 30° is shown in Figure 47. The time divisions are 50 psec. The first pulse is the pulse radiated from the back of the TEM horn. The main radiated on-boresight pulse is not visible to the probe at this angle. The second pulse is the field diffracted from the edge. The exponential taper outperforms the triangular taper. The actual decrease is very slight, only about 1 dB. Notice the time shift of the diffracted field due to the longer length of the horns with the TPS attachments.

59

Off Boresight (30 degrees)
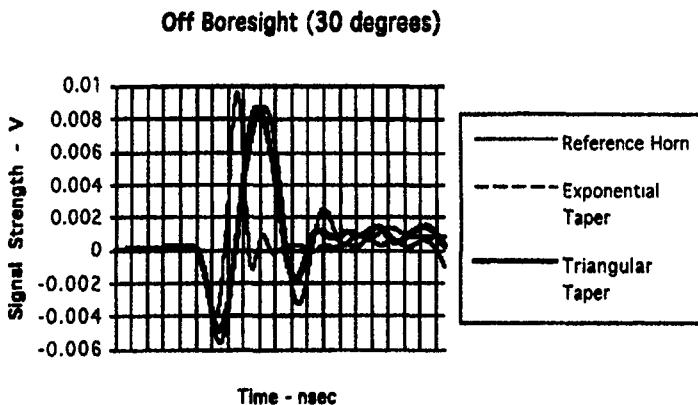
Figure 47. Electric Fields Impulse Response at
30° Off Boresight for the Reference Horn,
Exponential Taper, and Triangular Taper

The impulse response for the fields off-boresight 60° is depicted in Figure 48.
The time divisions are again 50 psec. The reference horn trace shows the pulse coming
from the back of the horn and the pulse diffracted at the edge. The taper traces show only
the diffracted fields. The added length of the TPS made it impossible to show the pulse
from the source. The diffracted fields spread appreciably this far off the boresight. This
is not a problem since the goal is to reduce the peak levels. The exponential taper reduces
the field levels further than the triangular taper.

60

Off Boresight (60 degrees)
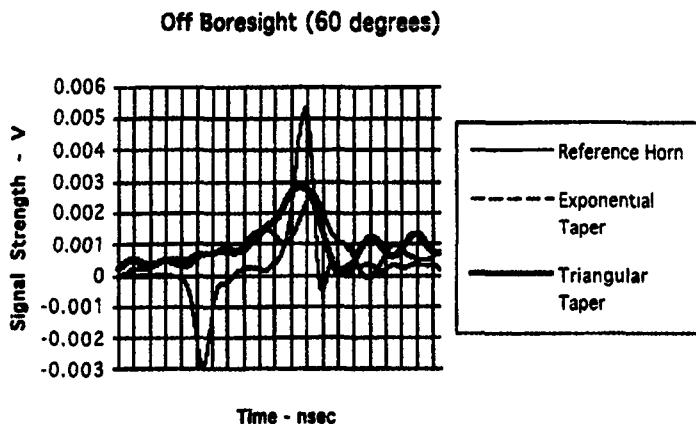
Figure 48. Electric Fields Impulse Response at
60° Off Boresight for the Reference Horn,
Exponential Taper, and Triangular Taper

The traces in Figure 49 show the impulse response 90° off the boresight. The time divisions are 50 psec. The time delay between the pulse escaping from the back of the horn and the pulse diffracted from the edge is too great to be placed on the same axes. The plot shows only the fields diffracted from the edges. The traces are shifted in the post processing; therefore, nothing can be interpreted from the time positions of the traces.

61

Off Boresight (90 degrees)
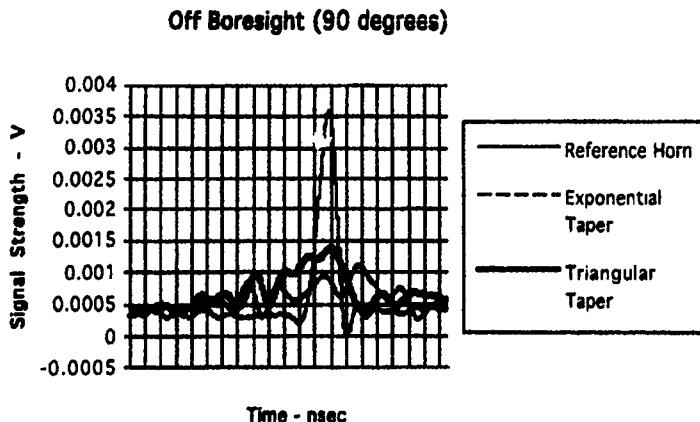
Figure 49. Electric Fields Impulse Response at
90° Off Boresight for the Reference Horn,
Exponential Taper, and Triangular Taper

Again the tapers reduce the peak electric field levels. The exponential
outperforms the triangular taper by approximately 1.8 dB. The tapers perform the best
when far off the boresight. This is supported by not only the FDTD modeling but also
past research [10].

The above plots are only a few examples of the performed measurements.
Appendix D contains plots of all the measurements.

Table 2 displays the peak values of the fields at each location and the amount of
reduction performed by each taper. The first column, Test Pt., gives the test location for
each measurement. The second row pulse, is the main radiated pulse. Ideally, the taper
measurements are higher than the reference horn measurements. The other measurements

62

ADA289708

are the diffracted field levels. The signal level is measured in millivolts. The reduction, in dB, is calculated as follows:

$$\text{Reduction (dB)} = 20 \log\left(\frac{V_{peak, taper}}{V_{peak, ref}}\right). \tag{20}$$

Test Pt.	Ref. Horn (mV)	Exp. Taper (mV)	Reduction (dB)	Tri. Taper (mV)	Reduction (dB)
pulse	13.1700	9.86849	-2.507	9.11670	-3.195
0°	-8.87810	-6.03380	-3.354	-6.69750	-2.448
20°	5.34938	6.12187	+1.172	5.22781	-0.200
30°	9.63531	8.82187	-1.381	8.65000	-0.937
40°	8.78906	5.79719	-3.614	7.08406	-1.873
50°	6.59125	3.67563	-5.073	4.54060	-3.237
60°	5.31500	2.58125	-6.273	2.82281	-5.496
70°	4.61313	1.77188	-8.311	2.28313	-6.109
80°	3.94125	1.36625	-9.202	1.64688	-7.591
90°	3.57531	1.12438	-10.048	1.37875	-8.277

Table 2. Test Results of the Peak Field Levels of the Exponential
and Triangular Taper Relative to the Reference Horn

The exponential taper outperforms the triangular taper at all locations except the 20° off-boresight test point. Even for the on-boresight maximization that did not behave as expected, the exponential taper approached the goal more closely than the triangular taper. The 20° off-boresight mark is a confusing point. Since that is the angle of elevation of the TEM horn, the location corresponds to grazing incidence for the radiating pulse and any diffraction occurring at the edge. Diffraction is very weak near grazing and is difficult to predict accurately. The discrepancy at this location is due to slight shifts in the probe location.

63

Summary

There were six sections in this chapter. The first section gave the results of the TEM horn model. The results of the PMM modeling and design were detailed in the second section. The sheet impedance of the taper elements was described in the fourth section. The fifth section detailed the approximate impedance functions at frequencies other than the design frequency. The final section described the results of the testing performed in this thesis.

64

Chapter 5: Conclusions and Suggestions

This chapter recaps the conclusions of this thesis research and provides some suggestions for follow-on work. The major conclusions for each main part of the design are discussed. A method for optimization is presented along with other suggestions.

Conclusions

The research in this thesis is detailed in previous chapters. Chapter 3 provides a description of the theory and design of the TEM horn antenna and TPS structures. Chapter 4 provides a description of the results of the design and testing. This section briefly recaps the results and provides some conclusions.

TEM Horn Design

The TEM horn design performs as expected. The reference horn provides the basis for this conclusion. The testing shows the radiation of the bandwidth of interest (300 MHz to 6 GHz). The field level decreases off-boresight demonstrating the directivity of the horn. Therefore, it is reasonable to conclude the design equations are valid.

TEM Horn Modeling

The model of the TEM horn is very approximate. Computer memory and calculation speed dictate the highest level of modeling. For example, the approximate model takes four days on an Indigo Silicon Graphics workstation. The stair stepping errors limit the bandwidth to half of the desired bandwidth.

The results of the models are not very enlightening. The horn radiates the source and sampling the off-boresight fields shows the directivity of the horn. However, the source is only a fraction of the designed operational bandwidth. To accomplish a more complete model requires better computational facilities.

65

TPS Design

The TPS designs perform as expected. The tapers reduce the off-boresight fields when compared to the reference horn. The TPSs provide a smooth transition from the conductive elements of the horn to free space. The approximate impedance functions sufficiently fit the desired impedance functions. The reflection coefficient changes along the length of the taper to gradually increase the impedance along the length.

TPS Modeling

The TPS modeling is only adequate to provide a qualitative level of field reduction. Computational limitations allow the tapers to be modeled only in two dimensions. The relative reduction in diffracted field levels determined by the performance of each taper compared to a reference plate provides a method to rank relative field reduction. The amount of reduction from each simulation does not correspond to the amount of reduction in the actual taper due to the two-dimensional limitation.

FDTD Simulation Responses
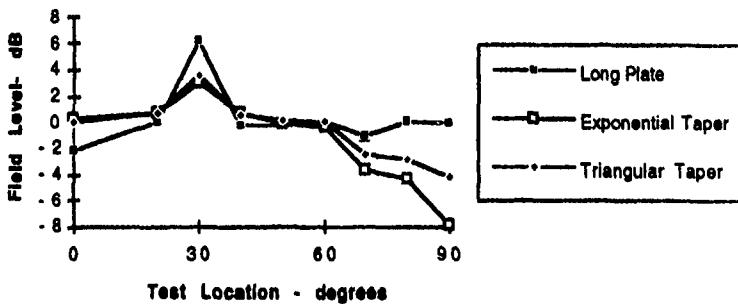
Figure 50. FDTD Simulation Field Level Relative to the
Field Diffracted from the Reference Horn
(Exponential Taper, Triangular Taper, and Long Plate)

66

ADA289708

FDTD Simulation Responses
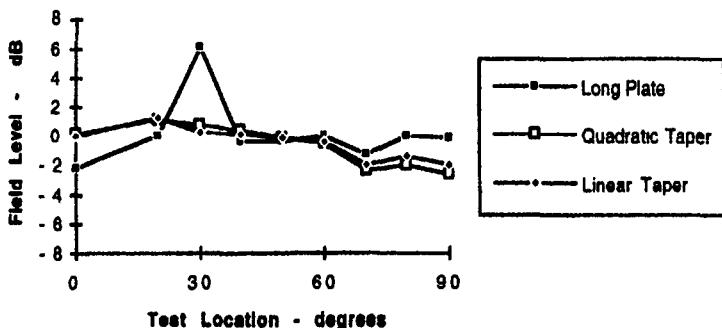
Figure 51. FDTD Simulation Field Level Relative to the
Field Diffracted from the Reference Horn
(Linear Taper, Quadratic Taper, and Long Plate)

The above plots, shown in Figures 50 and 51, demonstrate the predicted ability of
the tapers to reduce the diffracted field levels. The long plate is plotted on both figures to
provide a common measure. The long plate is the best solution for the angles closest to the
boresight. All the tapers provide better reduction than the long plate for angles beyond 20°.
According to the FDTD predictions the exponential taper provides the best reduction. The
triangular taper decreases the fields more than the quadratic and linear taper. Therefore, the
FDTD simulation suggests that the two best tapers are the exponential and triangular tapers.

The possibility of full three-dimensional modeling was examined. The problem
space requires 4210 × 1500 × 1082 cells. This translates to 6.8 billion vector unknowns.
Currently, a Cray supercomputer cannot perform that many calculations in a reasonable
amount of time. Therefore, a two-dimensional model is the best simulation of the taper.

Testing Procedure

The test procedure confirmed the predictions of the models. The models predicts
the triangular taper would reduce the field levels compared to the reference horn The

67

models also predict the exponential taper will outperform the triangular taper. Both these expectations are verified by experiment.

The tapers meet the goal to reduce the off-boresight field levels. Unfortunately, the tapers do not meet the second goal to maximize the on-boresight peak levels. However, the project is still successful. The reduction of radiated pulse is only 2.507 dB for the exponential taper. The off-boresight fields are reduced more than 3.5 dB for most sample points. The triangular taper has similar successes. The reduction of the radiated pulse is 3.195 dB. Most off-boresight field levels are reduced by more than 2 dB.

Suggestions for Continued Research

While this thesis meets the majority of the goals, there are many areas that can be improved. The design of the TEM horn does not appear to need any change, but the modeling requires much work. The design of the TPS is still a very new and exciting topic; many possibilities still exist. In the future, full three-dimensional modeling may be possible to facilitate the design process.

The TEM horn FDTD model can be improved. A tighter fit to the actual geometry is possible. A conformal grid FDTD code eliminates the stair step errors. This allows the TEM horn to be entered as a single PEC slab. A conformal grid FDTD code allows analysis of the performance of the TEM horn over the full design bandwidth.

TPS elements of conductive strips are chosen for two main reasons. Previous work demonstrates that conductive strips reduce diffraction [10]. The other determining factor in the choice of TPS element is the computer modeling. The strips can be modeled in two dimensions. Current computer facilities do not support three-dimensional modeling.

There are other TPS elements. Other applications use slots, wires, three-legged, and four-legged elements. The choice of element offers distinct characteristics to the design of the TPS. The three-legged element, for example, is polarization insensitive. Computer modeling tends to be the limiting factor. Most elements require three-dimensional computer modeling.

68

Refining the TPS design process produces better fits to the desired impedance functions. The gaps are varied to produce the varying impedance. The gaps width changes in increments of 0.01 inches. The manufacturing tolerances allow 0.005 inches. Designing more elements provides a larger pool of elements from which to select.

Four impedance functions are developed — linear, quadratic, exponential, and triangular. Pozar [11] gives another taper which optimizes both bandwidth and performance. The Klopfenstein taper is similar to a stepped Chebyshev transformer has an impedance function is

$$\ln(Z(d)) = \frac{1}{2}\ln Z_0 Z_L + \frac{\Gamma_o}{\cosh A} A^2 \phi(\frac{2d}{L} - 1, A) \quad \text{for } 0 \leq d \leq L$$

$$\phi(x, A) = \int_0^x \frac{I_1\left(A\sqrt{1-y^2}\right)}{A\sqrt{1-y^2}} dy \quad \text{for } |x| \leq 1$$

$$\Gamma_o = \frac{1}{2}\ln\left(\frac{Z_L}{Z_o}\right)$$

$$A = \cosh^{-1}\left(\frac{\Gamma_o}{0.002}\right)$$

(21)

where I_1 is the modified Bessel function and Z_L is the maximum impedance at the free space end of the taper.

The final suggestion is to optimize the current design. The design of the TPS is the area in which the greatest optimization can occur. In the design of a conductive strip TPS, there are four defining parameters — the strip width, the gap width, the number of layers, and the thickness of the dielectric slab. The current design optimizes the reflection coefficient with respect to the gap width. The other parameters are chosen such that the performance meets the design criteria.

Optimization is a tedious process. Deciding on the measure of optimization is the first step. The obvious choice for TPS optimization is the reflection coefficient. A popular optimization scheme determines the reflection coefficient at two values for each of the defining parameters while holding the other parameters constant. Connecting the values of the reflection coefficient forms a plane. The steepest level of increase determines the

69

variable that affects the reflection coefficient the most. This variable is changed to produce another value of the reflection coefficient. The process continues until a peak is found.

For example, the reflection coefficient is found for two values of gap width, δ_1 and δ_2, and thickness, t_1 and t_2. Connecting the four values forms a plane as shown in Figure 52. The steepest slope determines which variable has the most affect on the reflection coefficient. In this case the thickness affects the reflection coefficient more than the gap width. Therefore, another reflection coefficient is found for a third thickness, t_3. The process continues until a n-th thickness leads to a lower reflection coefficient which has a lower value than the preceding reflection coefficient. This determines the peak thickness.
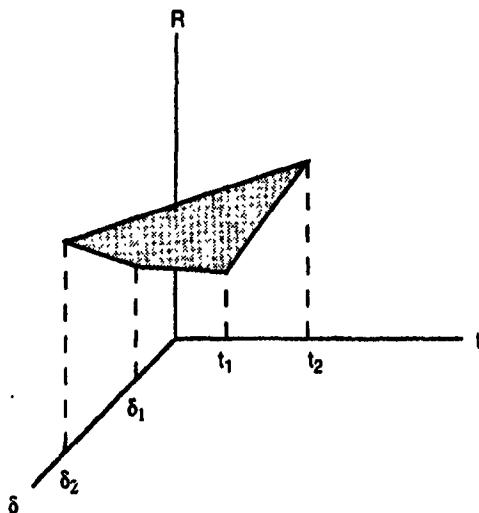
Figure 52. Visual Demonstration of Optimization
Process to Optimize the Reflection Coefficient
with Respect to the Gap Width and Thickness
of the Dielectric Slab

The optimization method previously explained does have some limitations. The process only finds local extrema. It has no way of determining global extrema. The

70

process also cannot determine if the system continually increases (or decreases). In a continually increasing system no maximum exists.

While the only optimized parameter in the current TPS design is the gap width, the effects of the other parameters are investigated. The strip width affects the bandwidth of the TPS. As the thickness increases, the capacitance increases. The dielectric substrates are available in many thicknesses. Increasing the number of layers also increases capacitance. The manufacturing process require adhering the multiple layers together with glue. The computer model becomes more complicated. Other dielectrics with different permittivity are also available.

The design process currently designs 59 elements and then curve fits to a desired impedance function. A better methodology designs each element to fit the desired impedance value. The desired impedance determines the corresponding reflection coefficient. The desired impedance function is perfectly fit.

Summary

This research involved the design, modeling, and testing of both a TPS and TEM horns. The goal was to reduce the off-boresight fields for a TEM horn and increase the peak-to-peak field levels on boresight. This was accomplished by applying a TPS to the free space end. The TPS reduced the diffraction from the free space end by providing a gradual transition from the conductive plates of the TEM horn to free space.

Two tapers were designed — one that approximated an exponential impedance function and one that approximated a triangular impedance function. Both reduced the off-boresight fields of the TEM horn. In most cases the exponential taper reduce the field levels further than the triangular taper. For example at the test location 90° off the boresight, the exponential taper reduced the field diffracted from the edge by 10 dB. The triangular taper reduced the fields by 8.2 dB.

Therefore, this research proved that a TPS are effective method of reducing diffraction. A procedure for designing a TPS to fit a specific impedance function was presented. A two-dimensional FDTD model predicted the tapers would reduce the

71

diffraction. Experimentation results verify the TPS's ability to reduce the peak off-boresight field levels for a TEM horn.

.

72
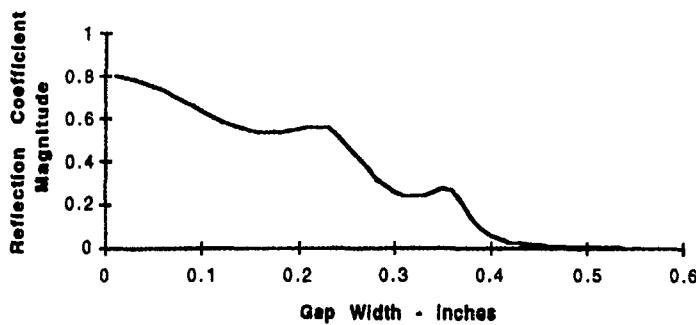
Reflection Coefficient vs. Gap Width at 300 MHz

Reflection Coefficient vs. Gap Width at 300 MHz

73
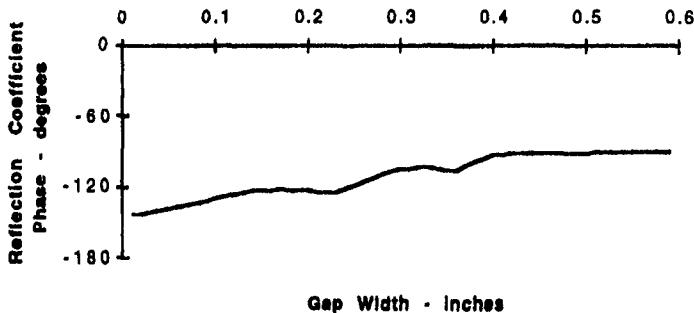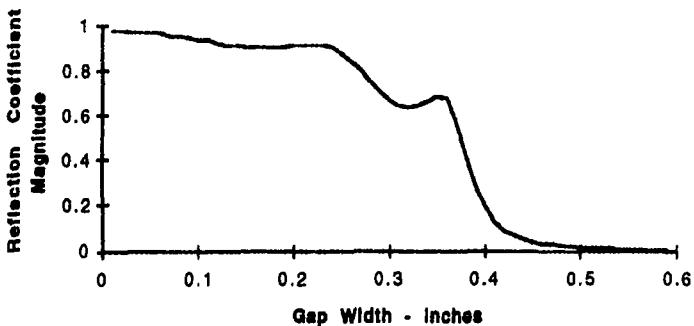
Reflection Coefficient vs. Gap Width at 1 GHz

Reflection Coefficient vs. Gap Width at 1 GHz

74
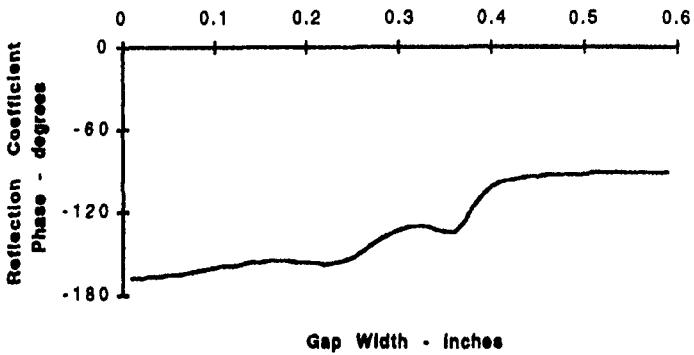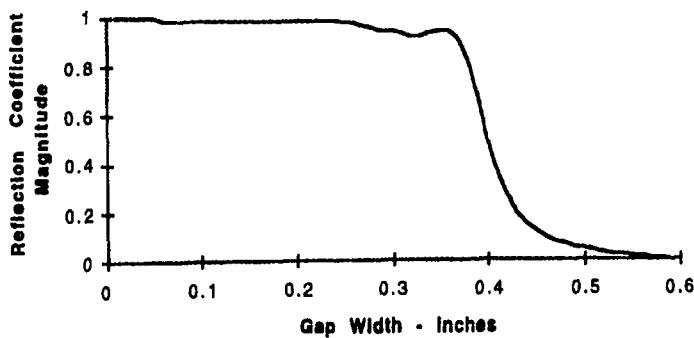
Reflection Coefficient vs. Gap Width at 3 GHz

Reflection Coefficient vs. Gap Width at 3 GHz
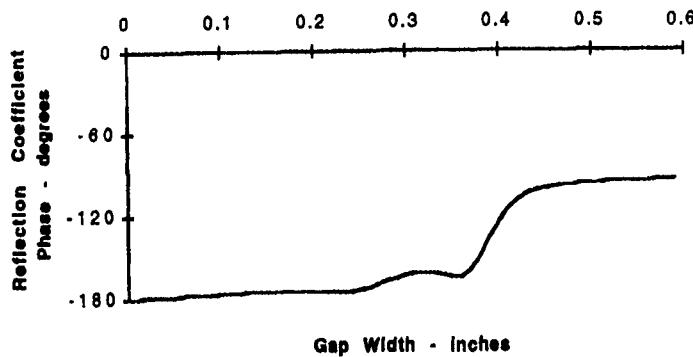
75

Reflection Coefficient vs. Gap Width at 6 GHz

Reflection Coefficient Magnitude vs. Gap Width - Inches

Reflection Coefficient vs. Gap Width at 6 GHz

Reflection Coefficient Phase - degrees vs. Gap Width - Inches

76
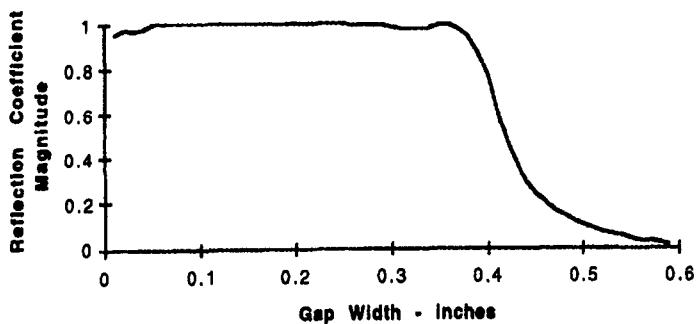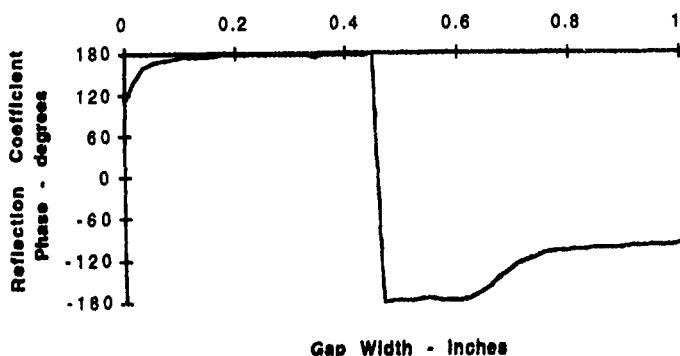
Appendix B

```
PROGRAM SHEETIMPEDANCE
 REAL HI,LO,MAG,PHASE,MAGNO,X,Y,FREQ,RES,REACT,ZMZG,ZPHS
 CHARACTER*80 LINE
 CHARACTER*5 FLAG /'--T--'/
 COMPLEX R,Z

 PI = ACOS(-1.)

 WRITE(*,*) 'LOW'
 READ(*,*) LO
 WRITE(*,*) 'HIGH'
 READ(*,*) HI
 WRITE(*,*) 'INCREMENT'
 READ(*,*) DF

 OPEN(UNIT=21,FILE='D99.OUT',STATUS='OLD')
 OPEN(UNIT=22,FILE='IMP99.DAT',STATUS='UNKNOWN')
 OPEN(UNIT=23,FILE='PHS99.DAT',STATUS='UNKNOWN')

 N=0
 DO 10, M=1,10000
  READ(21,FMT='(A)') LINE
  IF (LINE(29:33).NE.FLAG) GOTO 10
   READ(21,FMT='(A)') LINE
   READ(21,FMT='(A)') LINE
   READ(21,FMT='(A)') LINE
   READ(UNIT=LINE(65:69),FMT=*) MAG
   READ(UNIT=LINE(71:76),FMT=*) PHASE
   MAGNO=10**(MAG/20.)
   X=MAGNO*COS(PHASE*PI/180.)
   Y=MAGNO*SIN(PHASE*PI/180.)
   R=CMPLX(X,Y)
   Z=-377.*COS(80.*PI/180.)*((1.,0.)+R)/(2*R)
   N=N+1
   FREQ=(LO-DF)+DF*N
   RES=REAL(Z)
   REACT=AIMAG(Z)
   ZMAG=SQRT(RES**2+REACT**2)
   ZPHS=ATAN(REACT/RES)*180./PI
   WRITE(22,*) RES
   WRITE(23,*) REACT
  ENDIF

10 CONTINUE

 END
```

77.

Appendix C

Long Plate Scattered Field at 90 degrees

Long Plate Scattered Field at 80 degrees

79

Long Plate Scattered Field at 70 degrees

80

Long Plate Scattered Field at 60 degrees

81

Long Plate Scattered Field at 50 degrees

82

Long Plate Scattered Field at 40 degrees

83

Long Plate Scattered Field at 30 degrees

84

Long Plate Scattered Field at 20 degrees

85

Long Plate Scattered Field at 0 degrees

86

Quadratic Taper Scattered Field at 90 degrees

Quadratic Taper Scattered Field at 80 degrees

Quadratic Taper Scattered Field at 70 degrees

89

Quadratic Taper Scattered Field at 60 degrees

Quadratic Taper Scattered Field at 50 degrees

91

Quadratic Taper Scattered Field at 40 degrees

92

Quadratic Taper Scattered Field at 30 degrees

Quadratic Taper Scattered Field at 20 degrees

94

Quadratic Taper Scattered Field at 0 degrees

95

Linear Taper Scattered Field at 90 degrees

96

Linear Taper Scattered Field at 80 degrees

Linear Taper Scattered Field at 70 degrees

Linear Taper Scattered Field at 60 degrees

99

Linear Taper Scattered Field at 50 degrees

100

Linear Taper Scattered Field at 40 degrees

101

Linear Taper Scattered Field at 30 degrees

102

Linear Taper Scattered Field at 20 degrees

103

Linear Taper Scattered Field at 0 degrees

104

Exponential Taper Scattered Field at 90 degrees

105

Exponential Taper Scattered Field at 80 degrees

106

Exponential Taper Scattered Field at 70 degrees

107

Exponential Taper Scattered Field at 60 degrees

108

Exponential Taper Scattered Field at 50 degrees

109

Exponential Taper Scattered Field at 40 degrees

110

Exponential Taper Scattered Field at 30 degrees

111

Exponential Taper Scattered Field at 20 degrees

Exponential Taper Scattered Field at 0 degrees

113

Triangular Taper Scattered Field at 90 degrees

Triangular Taper Scattered Field at 80 degrees

115

Triangular Taper Scattered Field at 70 degrees

116

Triangular Taper Scattered Field at 60 degrees

117

Triangular Taper Scattered Field at 50 degrees

118

Triangular Taper Scattered Field at 40 degrees

119

Triangular Taper Scattered Field at 30 degrees

120

Triangular Taper Scattered Field at 20 degrees

121

Triangular Taper Scattered Field at 0 degrees

122

Reference Plate Scattered Field at 90 degrees

123

Reference Plate Scattered Field at 80 degrees

124

Reference Plate Scattered Field at 70 degrees

125

Reference Plate Scattered Field at 60 degrees

Reference Plate Scattered Field at 50 degrees

127

Reference Plate Scattered Field at 40 degrees

128

Reference Plate Scattered Field at 30 degrees

129

Reference Plate Scattered Field at 20 degrees

130

Reference Plate Scattered Field at 0 degrees

131

Appendix D

This appendix contains the results of the testing performed at the High Energy Research and Test Facility of Phillips Laboratory at Kirtland AFB, NM. There are three antennas tested — an all metal TEM horn (reference case), a horn with exponential taper attachment, and a TEM horn with a triangular taper attachment. The fields diffracted from each antenna are sampled at nine test points.

The following plots contain the traces of the diffracted fields for each test location. Each plot has two traces — one from each channel.

132

Reference Horn - On Boresight (0 degrees)

133
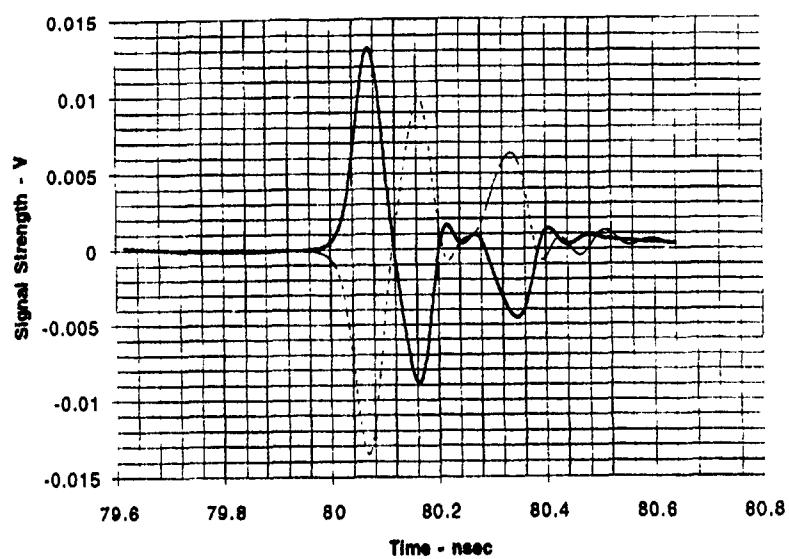
Reference Horn - Off Boresight (20 degrees)
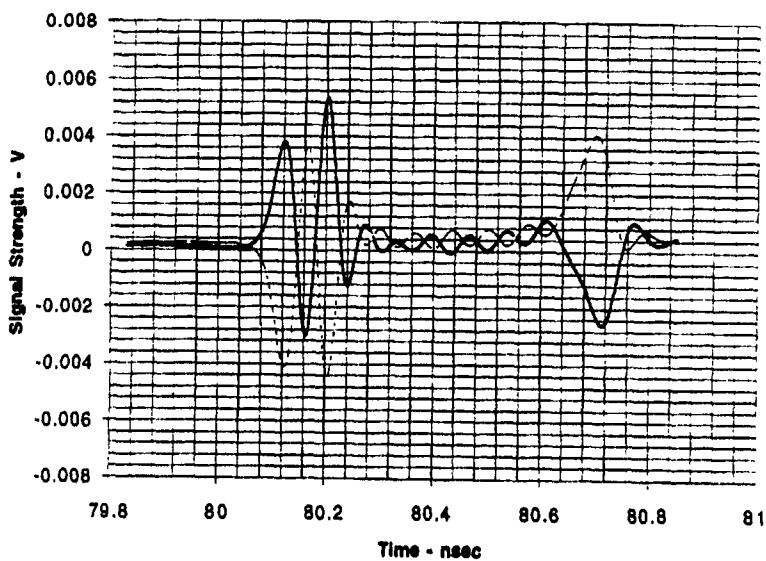
Reference Horn - Off Boresight (30 degrees)

135
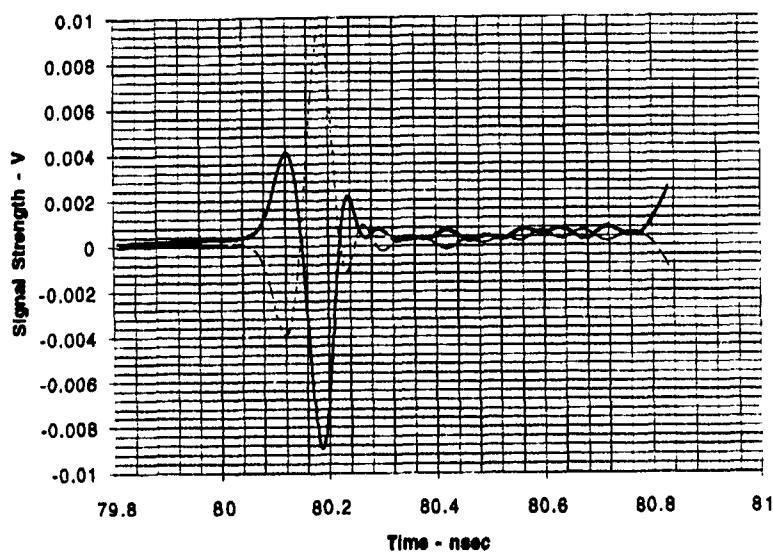
Reference Horn - Off Boresight (40 degrees)

136
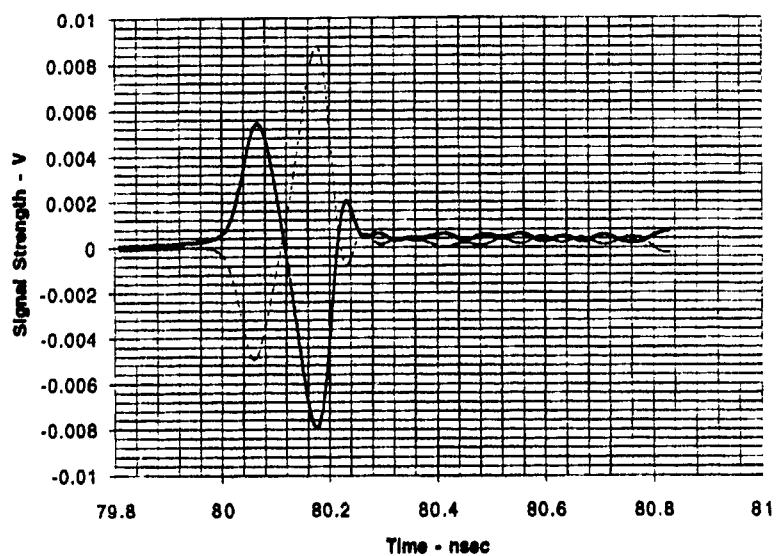
Reference Horn - Off Boresight (50 degrees)

137
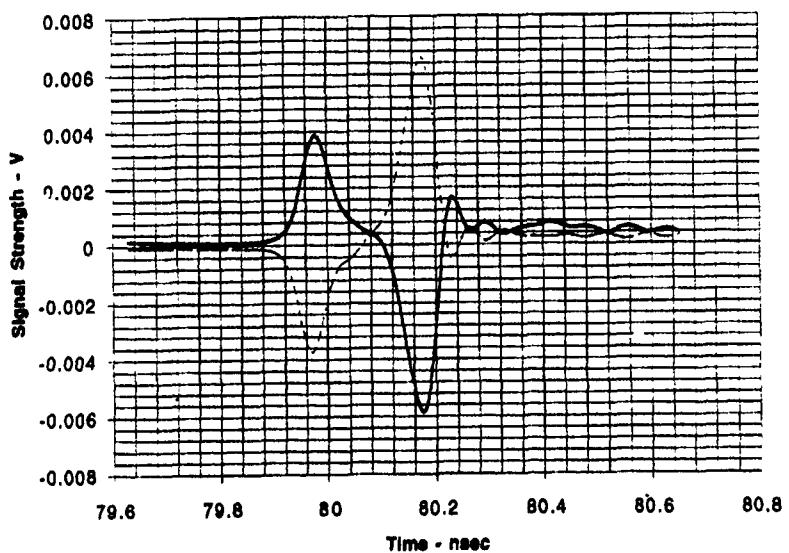
Reference Horn - Off Boresight (60 degrees)

138
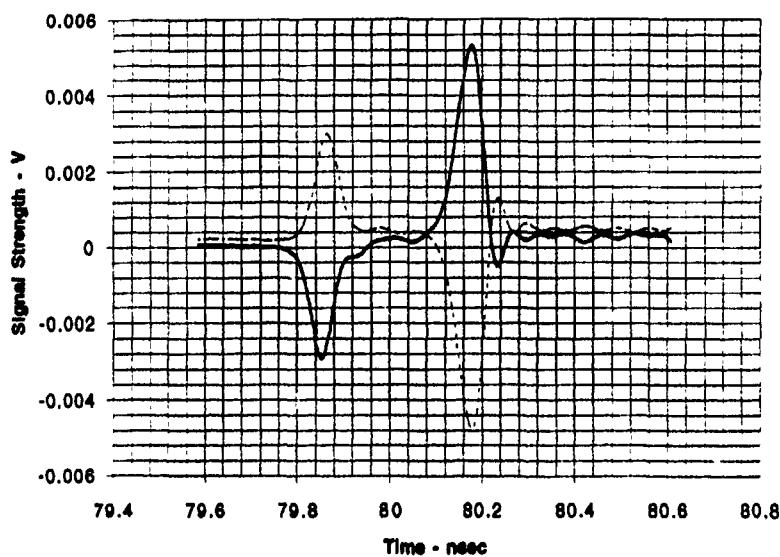
Reference Horn - Off Boressight (70 degrees)
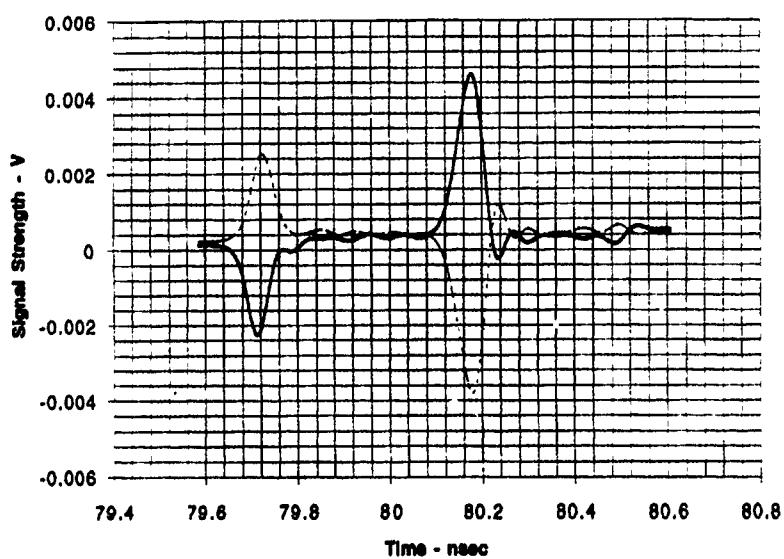
Reference Horn - Off Boresight (80 degrees)

140
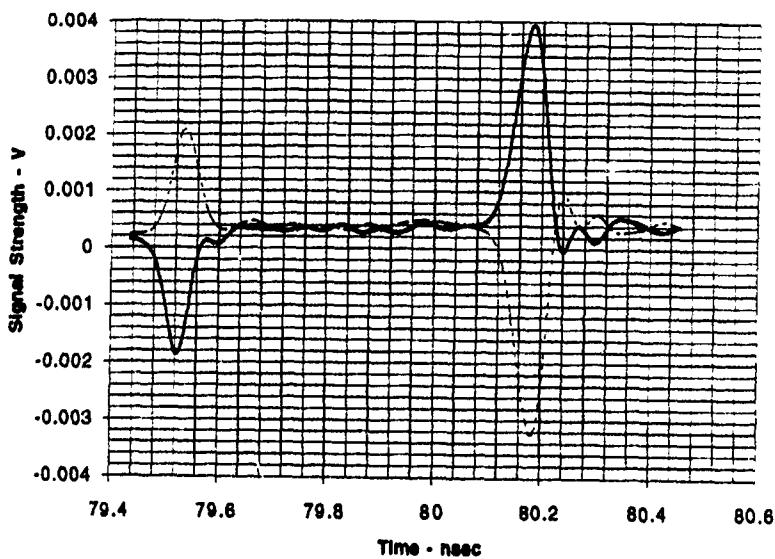
Reference Horn - Off Boresight (90 degrees)

141
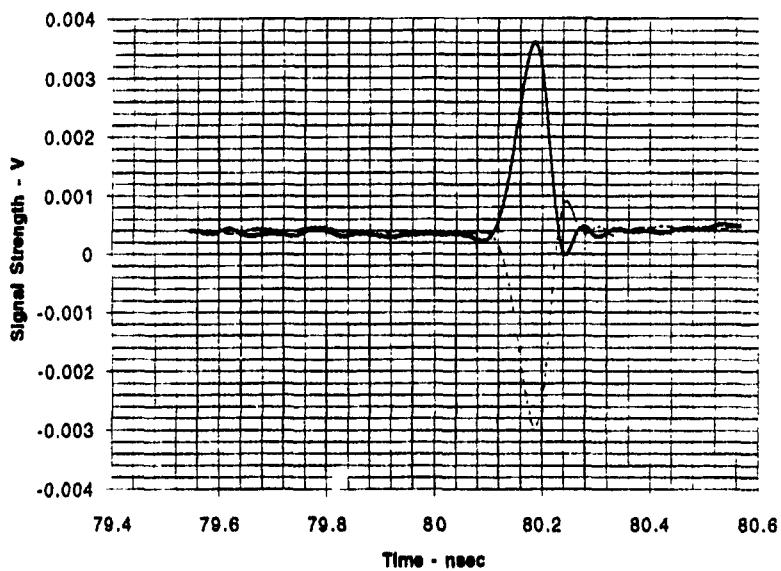
Triangular Taper - On Boresight (0 degrees)

142
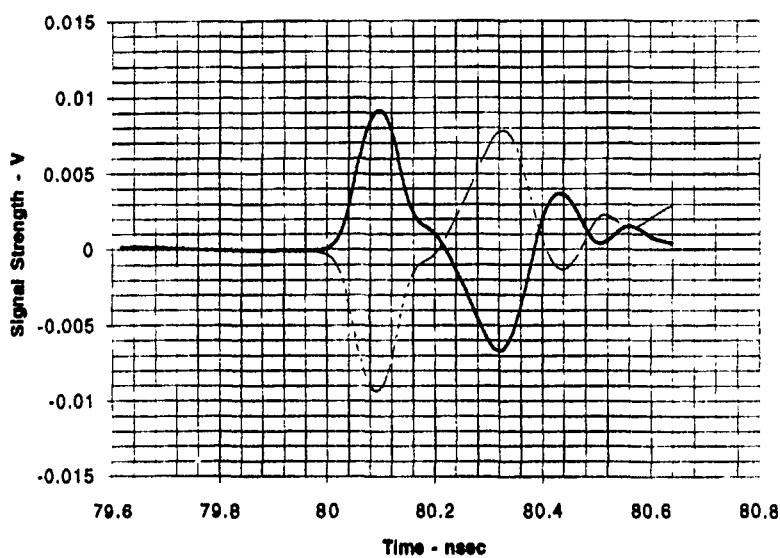
Triangular Taper - Off Boresight (20 degrees)

Triangular Taper - Off Boresight (30 degrees)


144
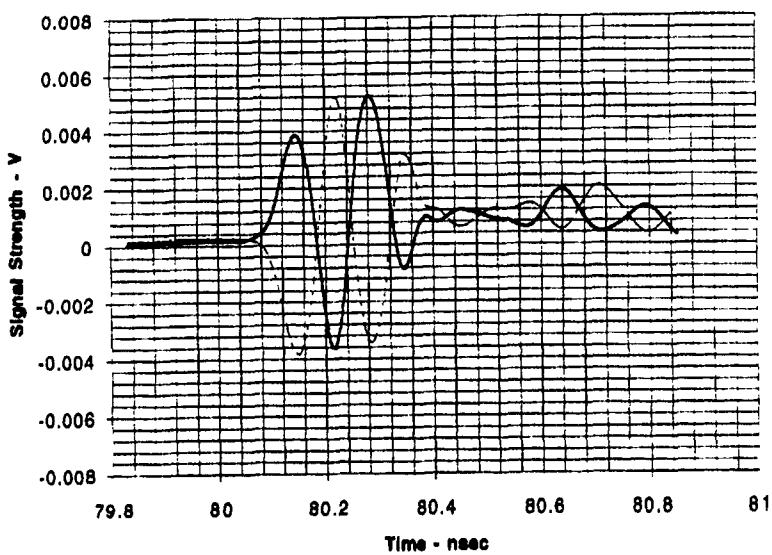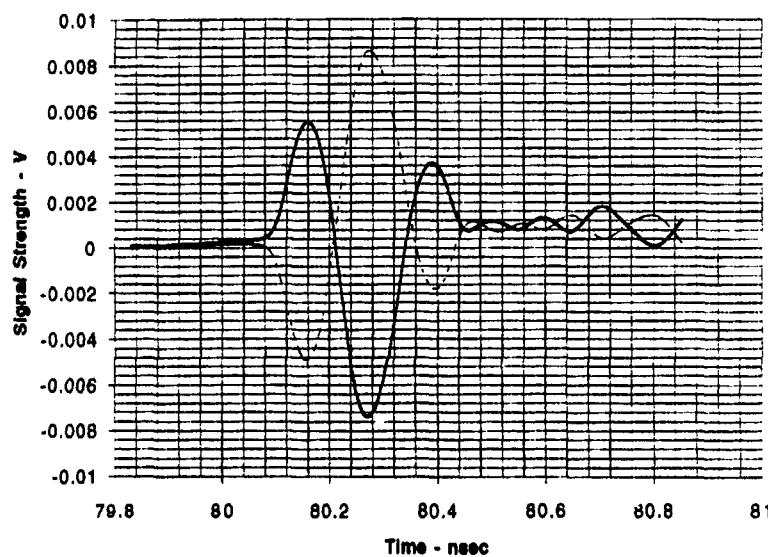
Triangular Taper - Off Boresight (40 degrees)

145
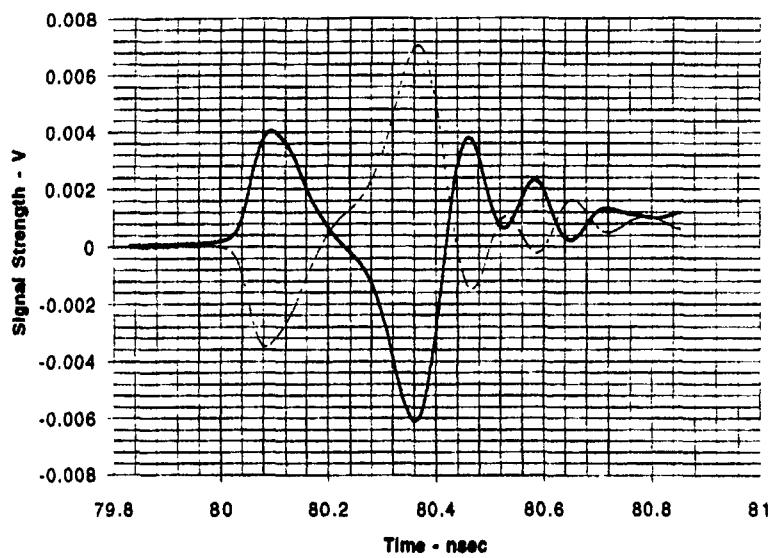
Triangular Taper - Off Boresight (60 degrees)

147
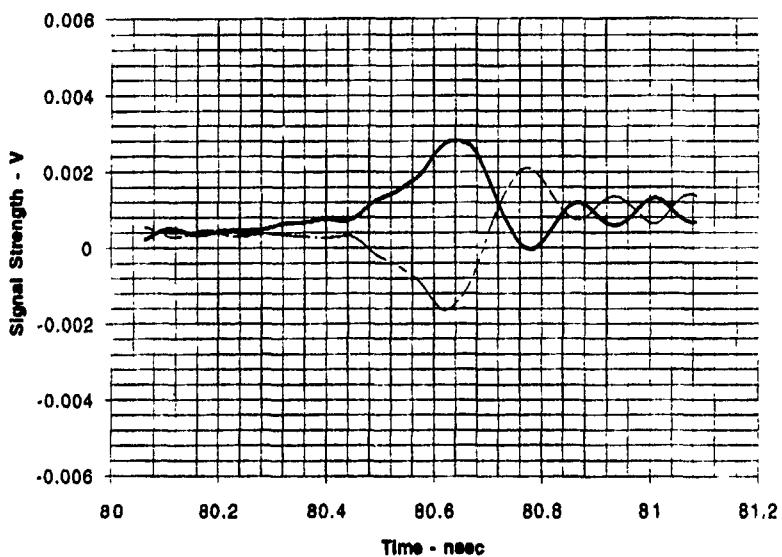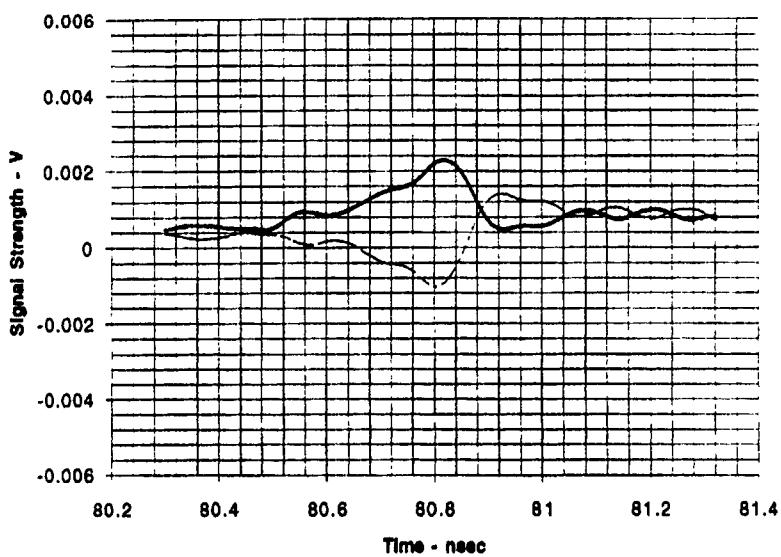
Triangular Taper - Off Boresight (70 degrees)

Triangular Taper - Off Boresight (80 degrees)

149

## Triangular Taper - Off Boresight (90 degrees)

150
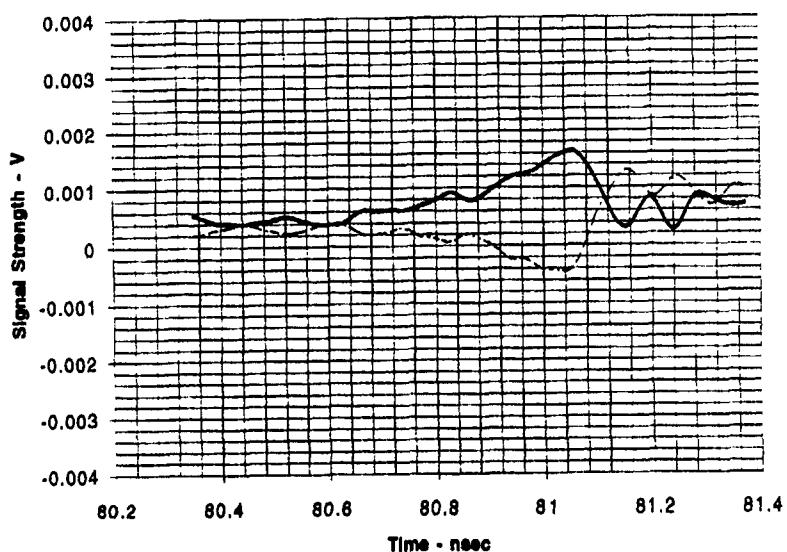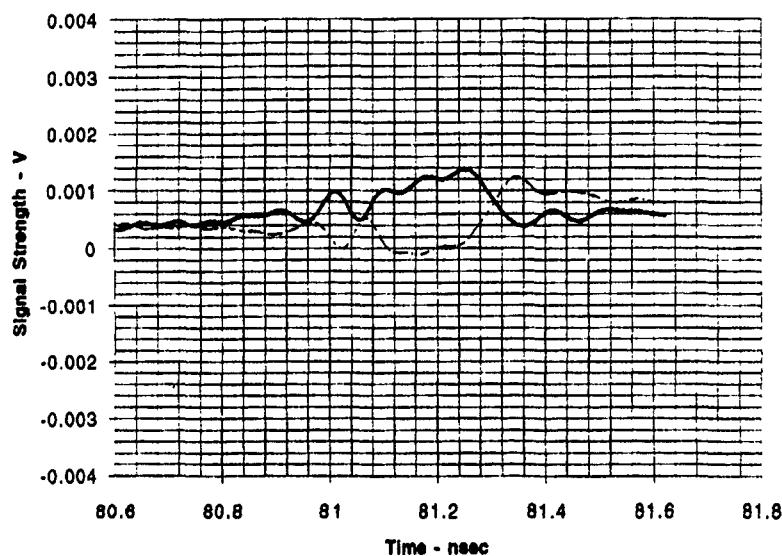
Exponential Taper - On Boresight (0 degrees)
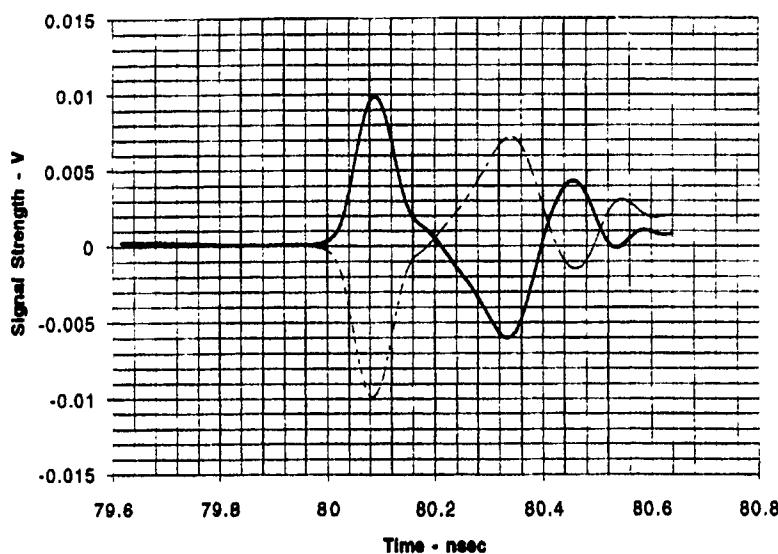
Exponential Taper - Off Boresight (20 degrees)

*Axis labels: Signal Strength - V (vertical), Time - nsec (horizontal)*

152

**Exponential Taper - Off Boresight (30 degrees)**


153
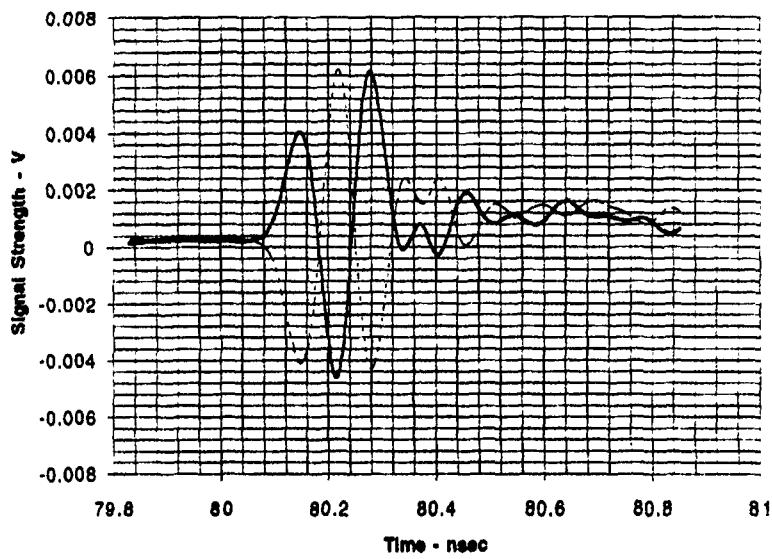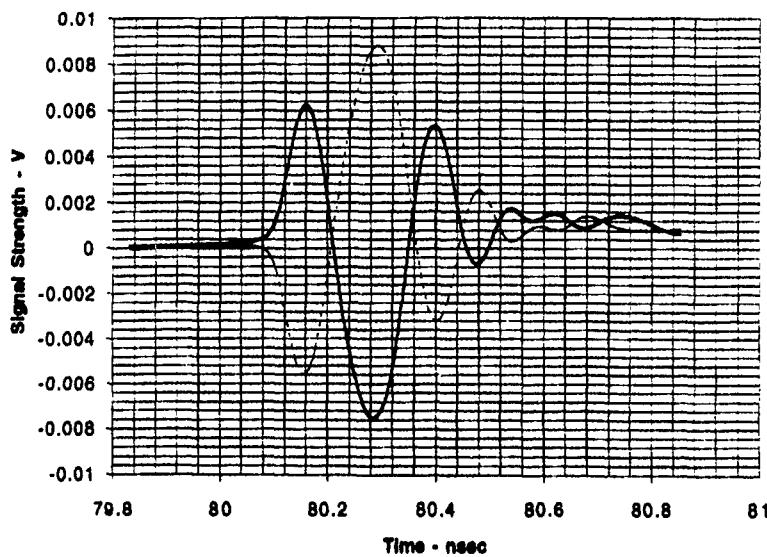
Exponential Tapers - Off Boresight (40 degrees)
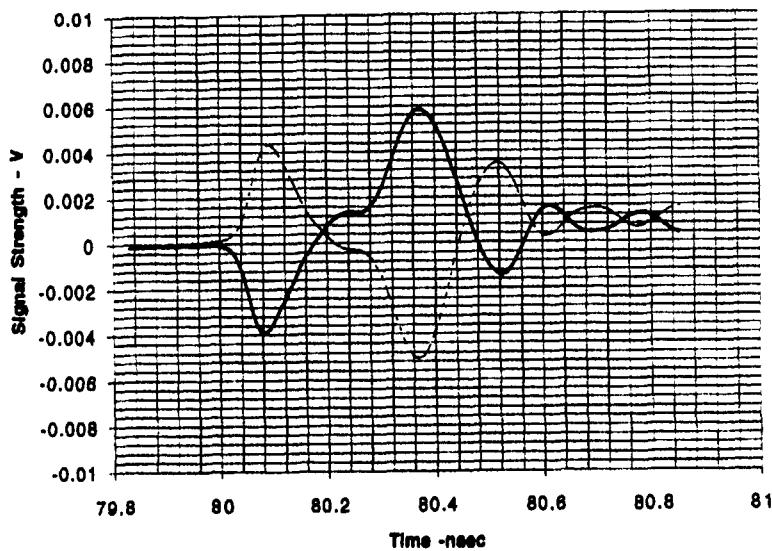
Exponential Taper - Off Boresight (50 degrees)
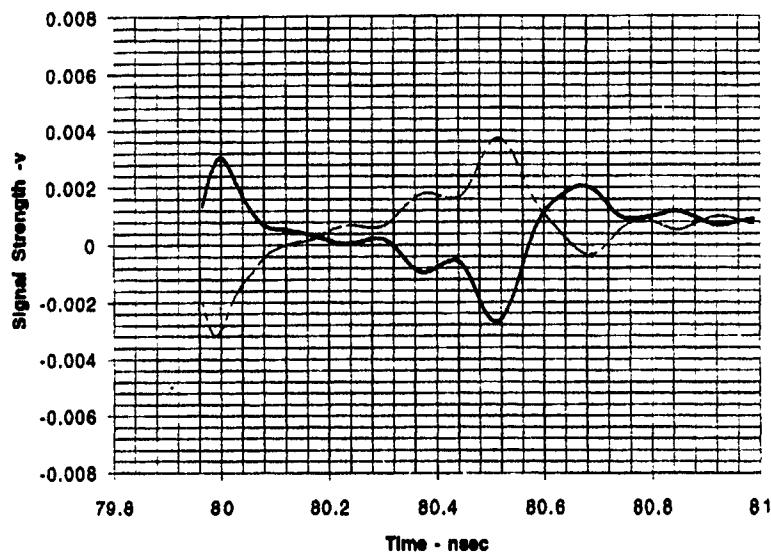
155

Exponential Taper - Off Boresight (60 degrees)

156

## Exponential Taper - Off Boresight (70 degrees)

157
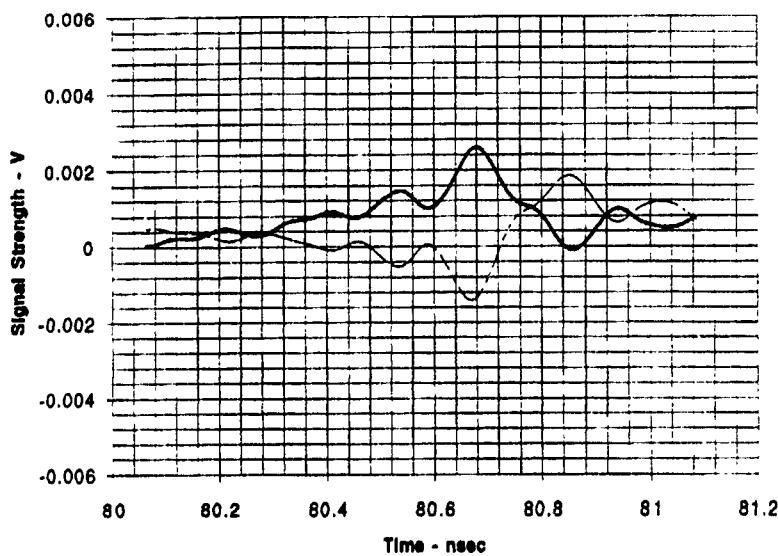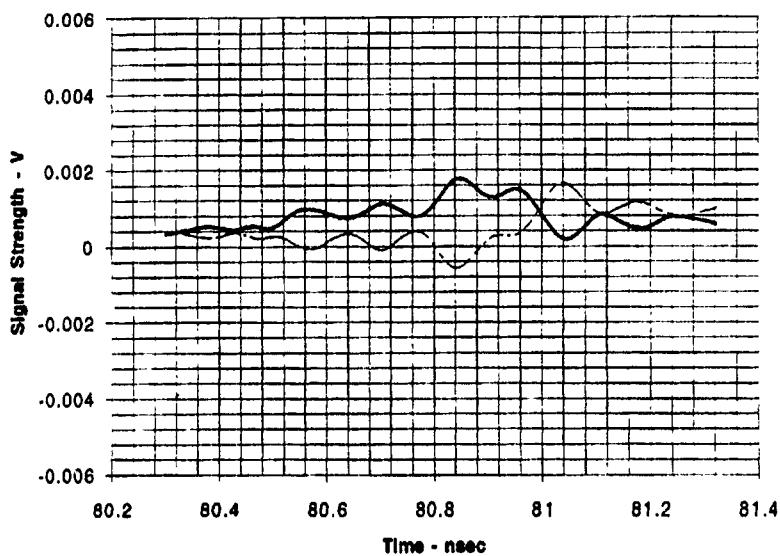
Exponential Taper - Off Boresight (80 degrees)
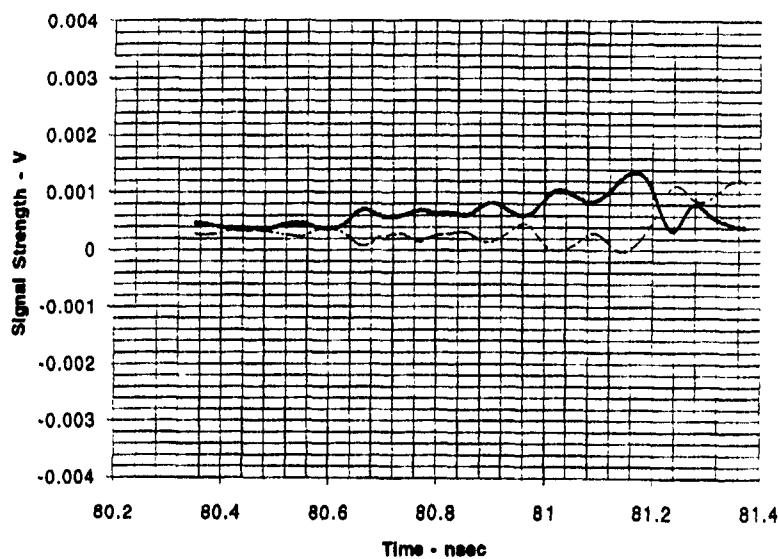
Exponential Taper - Off Boresight (90 degrees)
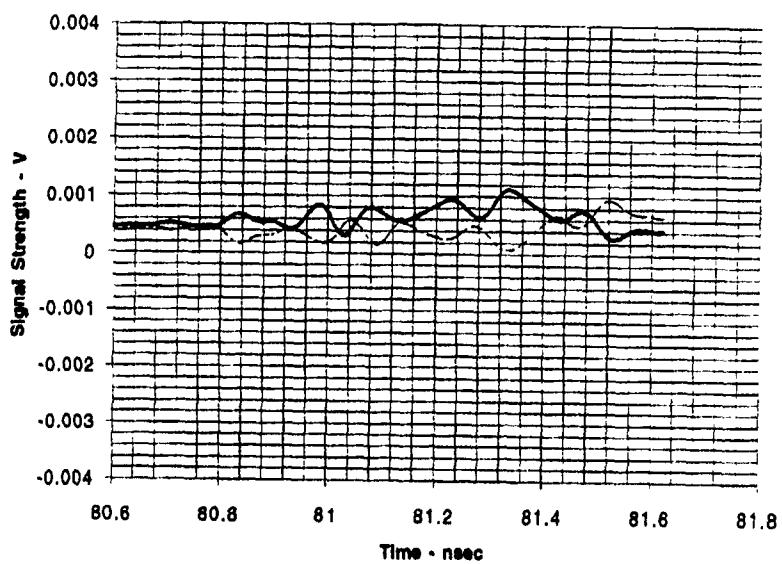
Bilbliography

[1] S. Evans and F. Kong. "TEM Horn Antenna: Input Reflection Characteristics in Transmission," *IEE Proc.*, Vol. 130, Pt. H, No. 6, pp. 403-409. Oct. 1983.

[2] E. K. English, inventor. *Tapered Periodic Surface*. Description of Invention for Patent Application. Dayton:EM Observables, Mission Research Corporation, January 22, 1990.

[3] K. S. Kunz and R. J. Luebbers, *The Finite Difference Time Domain Method for Electromagnetics*, CRC Press, Boca Raton, FL, 1993.

[4] L. W. Henderson, *Introduction to PMM Version 3.0*. The Ohio State University, EletroScience Laboratory, Columbus, OH, 1989.

[5] A. R. Ondrejka, J. M. Ladbury, and H. W. Medley, "TEM Horn Antenna Design Guide," National Institute of Standards and Technology, unpublished report.

[6] W. E. Stutzman and G. A. Thiele. *Antenna Theory and Design*. New York: John Wiley & Sons, 1981.

[7] M. Kanda, "The Effects of Resistive Loading of "TEM" Horns," *IEEE Trans. Electromagn. Compat.*, Vol. EMC-24, No. 2, pp 245-255, May 1992.

[8] J. G. Maloney. *Analysis and Synthesis of Transient Antennas using the Finite Difference Time Domain (FDTD) Method*. PhD dissertation. Georgia Institute of Technology, Atlanta, GA, 1992.

[9] E. K. English. "Tapered Periodic Surfaces: A Basic Building Block for Broadband Antenna Design," *Proceedings from the Second International Conference on Ultra-Wideband, Short Pulse Electromagnetics*. not yet published.

[10] R. A. Burleson. *A Study of Two Dimensional Tapered Periodic Edge Treatments to Reduce Wideband Diffraction*. MS Thesis, AFIT/GE/ENG/93D-02. School of Engineering, Air Force Institute of Technology (AETC), Wright-Patterson AFB OH, December 1993.

[11] D. M. Pozar. *Microwave Engineering*. Reading, Mass:Addison-Wesley Publishing Company, 1990.

[12] J. H. Beggs, R. J. Leubbers, and H. S. Langdon. *User's Manual for TEC: PSU FDTD Code Version C for Two-Dimensional Transverse Electric Transient Scattering from Frequency-Independent Dielectric and Magnetic Materials*. Electrical and Computer Engineering Department, The Pennslyvania State University, University Park, PA, June 1993.

[13] F. G. Stremler. *Introduction to Communication Systems*. Reading, Mass:Addison-Wesley Publishing Company, 1990.

Vita

Second Lieutenant Dennis J. Wolstenholme was born on 24 Jan, 1971 in Arlington Virginia. He graduated from Paul VI High School in 1989. He attended Virginia Polytechnic Institute and State University and graduated with a degree in Electrical Engineering in 1993. His first assignment was to the School of Engineering, Air Force Institute of Technology in Jun, 1993.

Permanent Address: 14014 Giles Street.
Woodbridge, VA 22191